JOURNAL OF PETROLOGY | VOLUME 48 | NUMBER 6 | PAGES 1119–1154 | 2007 | doi:10.1093/petrology/egm012

Origin of CFB Magmatism: Multi-tiered Intracrustal Picrite–Rhyolite Magmatic Plumbing at Spitzkoppe, Western Namibia, during Early Cretaceous Etendeka Magmatism

R. N. THOMPSON[1]*, A. J. V. RICHES[1†], P. M. ANTOSHECHKINA[2], D. G. PEARSON[1], G. M. NOWELL[1], C. J. OTTLEY[1], A. P. DICKIN[3], V. L. HARDS[4], A.-K. NGUNO[5] AND V. NIKU-PAAVOLA[5‡]

[1]DEPARTMENT OF GEOLOGICAL SCIENCES, DURHAM UNIVERSITY, SOUTH ROAD, DURHAM DH1 3LE, UK

[2]DIVISION OF GEOLOGICAL AND PLANETARY SCIENCES, CALIFORNIA INSTITUTE OF TECHNOLOGY, MC 170-25, PASADENA, CA 91125, USA

[3]DEPARTMENT OF GEOLOGY, MCMASTER UNIVERSITY, 1280 MAIN STREET WEST, HAMILTON, ONTARIO, CANADA L8S 4M1

[4]BRITISH GEOLOGICAL SURVEY, KEYWORTH, NOTTINGHAM NG12 5GG, UK

[5]GEOLOGICAL SURVEY OF NAMIBIA, 1 AVIATION ROAD, PRIVATE BAG 13297, WINDHOEK, NAMIBIA

RECEIVED FEBRUARY 22, 2006; ACCEPTED FEBRUARY 27, 2007
ADVANCE ACCESS PUBLICATION APRIL 28, 2007

Early Cretaceous tholeiitic picrite-to-rhyolite dykes around Spitzkoppe, western Namibia, are part of the extensive Henties Bay–Outjo swarm, penecontemporaneous with ~132 Ma Etendeka lavas ~100 km to the NW. Although only intermediate to rhyolitic dykes contain clinopyroxene phenocrysts, the behaviour of Ca, Al and Sc in the dyke suite shows that liquidus clinopyroxene—together with olivine—was a fractionating phase when MgO fell to ~9 wt %. Both a plot of CIPW normative di–hy–ol–ne–Q and modelling using (p)MELTS show that a mid-crustal pressure of ~0·6 GPa is consistent with this early clinopyroxene saturation. Sr, Nd, Hf and Pb isotope variations all show trends consistent with AFC contamination (assimilation linked to fractional crystallization), involving Pan-African Damara belt continental crust. The geochemical variation, including isenthalpic AFC modelling using (p)MELTS, suggests that the picrites (olivine-rich cumulate suspensions) were interacting with granulite-facies metamorphic lower crust, the intermediate compositions with amphibolite-facies middle crust, and the rhyolitic dykes (and a few of the basalts) with the Pan-African granites of the upper crust. The calculated densities of the magmas fall systematically from picrite to rhyolite and suggest a magmatic system resembling a stack of sills throughout the crust beneath Spitzkoppe, with the storage and fractionation depth of each magma fraction controlled by its density. Elemental and isotopic features of the ~20 wt % MgO picrites (including Os isotopes) suggest that their parental melts probably originated by fusion of mid-ocean ridge basalt (MORB) source convecting mantle, followed by limited reaction with sub-continental lithospheric mantle metasomatized just prior to the formation of the parental magmas. Many of the distinctive features of large-volume picritic–basaltic magmas may not be derived from their ultimate mantle sources, but may instead be the results of complex polybaric fractional crystallization and multi-component crustal contamination.

KEY WORDS: *flood basalts; Spitzkoppe; picrite; trace elements; hafnium isotopes; Etendeka*

INTRODUCTION

Attempts to understand the genesis and evolution of magmas can be subdivided into: (1) determining the physical and chemical conditions of magma genesis; (2)

*Corresponding author. E-mail: r.n.thompson@durham.ac.uk
†Present address: Department of Earth Sciences, The Open University, Walton Hall, Milton Keynes MK7 6AA, UK.
‡Present address: Directorate of Diamond Affairs, Ministry of Mines and Energy, 1 Aviation Road, Windhoek, Namibia.

understanding the processes that have affected the magmas between their genesis and final solidification. Researchers interested in the first process are inclined to see the second one as little more than a nuisance, standing between them and their objectives. For this reason it is common for such students of magmas to focus on samples, techniques or datasets that appear to them to evade the 'problem' of post-genesis processes. The flood basalts of large igneous provinces (LIPs) in general, and the early Cretaceous Paraná–Etendeka province in particular, have been and remain favourite battlefields for differing views about the relative importance of the two processes. The many publications that attempt to discern the ultimate sources of these magmas are split between favouring either the sub-continental lithospheric mantle (SCLM) or the underlying convecting mantle, with or without a contribution from either delaminated SCLM or older subducted material. Recent examples of such studies are those by Peate (1997), Ewart *et al.* (1998*a*, 2004*a*), Gibson *et al.* (2000, 2005), Marsh *et al.* (2001), Thompson *et al.* (2001), Trumbull *et al.* (2004*a*) and Tuff *et al.* (2005).

All these studies acknowledge the probability that hot upwelling magmas will react with and absorb relatively fusible continental crust. Some studies attempt to make allowances for such crustal contamination, usually by comparing the predicted chemical effects of a likely crustal contaminant, such as the local granite basement, with geochemical trends observed in the magmatic suite. Most published studies assume *a priori* that any such crustal contamination takes place by a process of assimilation linked to the fractional crystallization of the melt (AFC), such that magmas become progressively more contaminated with falling liquidus temperature. Hence, they routinely reverse this reasoning and propose that the best shortcut to identifying magmas that have undergone little or no reaction with continental crust is to focus only on those with relatively high MgO contents, and hence high liquidus temperatures.

This is difficult to do in the Paraná–Etendeka province. For example, the compendium of data by Peate (1997) shows almost no Paraná lava analyses with >7 wt % MgO. Likewise, Marsh *et al.* (2001) and Ewart *et al.* (2004*a*) showed that relatively few Etendeka lavas—excluding the basal ferropicrites (Gibson *et al.*, 2000)—have >9 wt % MgO. Even this higher MgO content falls far short of the lowest value calculated for melts to be in equilibrium with a peridotite mantle. Primary magmas do not fall below 13–14 wt % (Thompson *et al.*, 2005) and rise to values above 20 wt % MgO. Therefore all arguments that the elemental and isotopic variations in 'more Mg-rich' Paraná–Etendeka lavas are inherited from their mantle sources and unaffected by subsequent polybaric fractional crystallization and concomitant crustal contamination (e.g. Erlank *et al.*, 1984, and many subsequently) are, to some extent, acts of faith.

This study is concerned with a picrite–rhyolite suite of dykes exposed within the Etendeka igneous province, south of the lavas. They are approximately contemporaneous with the Etendeka extrusive rocks and often taken to be their hypabyssal equivalents (e.g. Marsh *et al.*, 1997; Trumbull et al, 2004*a*). All but one of these dykes shows clear geochemical evidence, detailed below, of reaction between the melts and the local continental crust. The only possible exception is one dyke with ~20 wt % MgO. The AFC reactions involved at least three distinctive crustal rock-types, at upper-, middle- and lower-crustal depths. Clinopyroxene precipitated, deep in the crust, when MgO in these fractionating melts reached ~9 wt % MgO. The combined effects of this process and the crustal contamination strongly affected many inter-element ratios in the magmas (including some routinely used to classify Paraná–Etendeka magma types), together with isotopes of Sr, Nd, Hf and Pb. This confirms other recent studies, which showed that, even when dealing with Mg-rich basalts and picrites (e.g. Kent *et al.*, 2002; Yaxley *et al.*, 2004; Saal *et al.*, 2005; Harlou *et al.*, 2006; Zhang *et al.*, 2006), post-genesis interactions between the upwelling melts and their surroundings are common.

SPITZKOPPE DYKE SWARM

The dyke swarm exposed in the Spitzkoppe area (Fig. 1) is part of the major Henties Bay–Outjo (HB–O) swarm (Lord *et al.*, 1996; Trumbull *et al.*, 2004*a*). The HB–O swarm mostly trends between NE–SW and NNE–SSW, and extends inland for at least 500 km from the continental margin. It forms part of the southern Etendeka Igneous Province (Marsh *et al.*, 2001). Whereas most Etendeka lavas are preserved in a belt adjacent to the Atlantic coast, dyke swarms and intrusive sub-volcanic centres extend inland within the Late Proterozoic to Cambrian Damara orogenic belt, along the southern margin of the Congo craton (Fig. 1, inset). The Cretaceous extension and magmatism of this region is generally considered to be an integral part of the igneous event that produced the Paraná–Etendeka lavas, more deeply eroded than the coastal belt (e.g. Milner & le Roex, 1996; le Roex & Lanyon, 1998; Marsh *et al.*, 1997, 2001; Wigand *et al.*, 2003). Trumbull *et al.* (2004*a*, fig. 1) defined the HB–O swarm as ~70 km wide in the vicinity of Spitzkoppe. To the NW there is a relatively narrow (~25 km) dyke-poor zone before reaching the dense parallel dyke swarm between the Cretaceous Brandberg and Messum intrusive complexes (Thompson *et al.*, 2001). For most of its length the HB–O dyke swarm is emplaced in metamorphic rocks—mica schists, migmatites, calc-silicates and marbles—and granites (*sensu lato*) of the Pan-African Damara belt but,

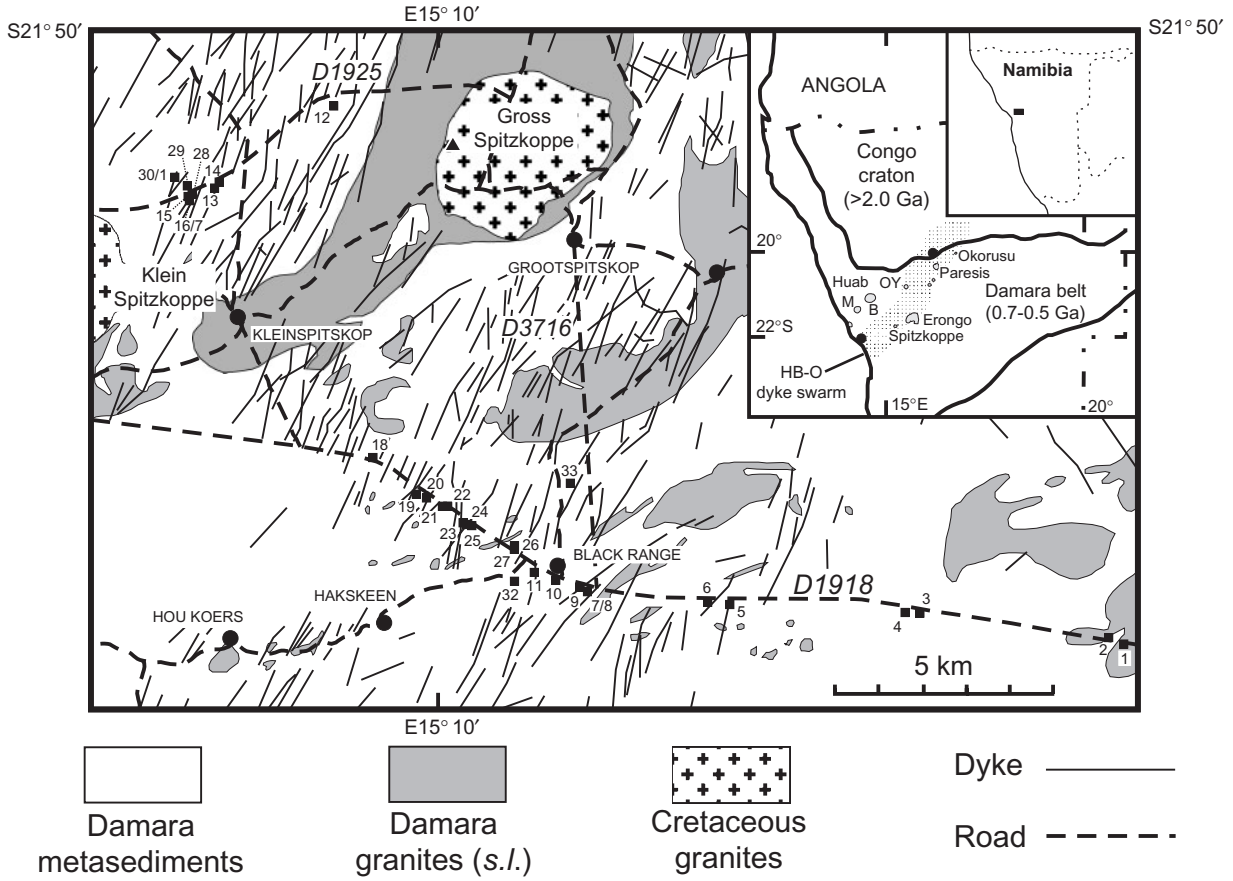

Fig. 1. Sketch map of the area around Spitzkoppe, western Namibia. Geology simplified after Geological Survey of Namibia (1997) and Frindt *et al.* (2004*b*). Areas of surficial cover (mostly pediment gravels and dune sands) are omitted, notable south of Klein Spitzkoppe. Numbered filled squares mark sampled dykes (apart from VB12 basement granite). Average trend of most sampled dykes is NNE. All sample numbers have the prefix VB. The Black Range picrite dyke forms a prominent topographic ridge SSW of sample VB32. Inset shows the location of the Henties Bay–Outjo (HB–O) dyke swarm, stippled, and some of the main early Cretaceous Etendeka intrusive complexes. M, Messum; B, Brandberg; OY, Okenyenya.

north of Outjo, it enters the Archaean–Proterozoic Congo Craton (Fig. 1, inset).

At first sight the possible maximum age of the HB–O dykes is only constrained geologically to be post-Damara, whereas their minimum age is constrained by the radiometric dates of the Cretaceous plutonic complexes that intersect them (Fig. 1, inset). Dykes of the Jurassic Karoo igneous province do not occur in central and NW Namibia. The closest Karoo dykes are at the NW extremity of the 179 Ma (Ar–Ar dates) Okavango giant dyke swarm, which terminates in NE Namibia—about 750 km NE of Spitzkoppe—and trends at a right angle to the HB–O swarm (Le Galle *et al.*, 2002). Trumbull *et al.* (2004*a*) discussed the age of the HB–O dykes in detail and noted that their only published radiometric dates were obtained using the K–Ar method and mostly fall in the range 116–143 Ma. All the HB–O dyke samples chemically analysed to date form a single coherent tholeiitic picrite–rhyolite suite (Marsh *et al.*, 1997; Trumbull *et al.*, 2004*a*; this paper). The picrite–intermediate compositions also occur in the abundant dykes SW of Brandberg and in the Huab and Horingbaai areas (Fig. 1, inset), where they intersect 133 Ma southern Etendeka basal lavas. Both they and the lavas are transected by the 131 Ma Brandberg intrusive complex (Thompson *et al.*, 2001). Immediately NE of Spitzkoppe the HB–O dykes are transected by the large Erongo central volcanic and intrusive complex (Fig. 1, inset), dated at 133–130 Ma (with errors ±0·8–1·9 Ma) by Wigand *et al.* (2003) using both Ar–Ar biotite and U–Pb zircon methods.

The Spitzkoppe swarm dykes cut Damara basement in the relatively flat surroundings of the prominent peaks formed by the Gross and Klein Spitzkoppe granite stocks (Fig. 1). They vary in width from 1 m to 10 m and their trends range from 10° to 90°, with most falling between 30° and 50°. Two of the picrites (VB19 and 32) occur as dykes between 20 m and >30 m thick; both form prominent topographic ridges.

Frindt *et al.* (2004*a*) and Trumbull *et al.* (2004*b*) both noted that felsic dykes are more common around

Spitzkoppe than elsewhere in the HB–O swarm, although they have the same trends as their mafic neighbours. On a regional scale, the Spitzkoppe granites appear to transect all the dykes and thus post-date them. Nevertheless, Frindt *et al.* (2004*a*) have shown that several of the mafic regional dykes penetrate the marginal granite. Within the granite, the mafic dykes have irregular margins and are cut by late-stage granitic veins. One mafic dyke also locally forms a zone of pillow-like enclaves within the granite. The chilled cuspate margins of the enclaves are typical of liquid–liquid magmatic contacts elsewhere and leave no doubt that the basic and acid melts coexisted (Frindt *et al.* 2004*a*; S. Frindt, personal communication, 2005). The whole-rock Rb–Sr isochron age of the Gross Spitzkoppe stock is 124·6 Ma ± 1·1 Ma (MSWD = 2·5), with initial $^{87}Sr/^{86}Sr = 0{\cdot}7134$ (Frindt *et al.*, 2004*b*) but this may be lower than the true emplacement and original cooling age, as a result of subsequent hydrothermal redistribution of Rb (S. Frindt, personal communication, 2005). A clear example of this hydrothermal redistribution of Rb in a pluton is the Beinn an Dubhaich granite, Skye, NW Scotland. Dickin (1980) obtained an Rb–Sr whole-rock isochron age for this pluton of 53·5 ± 0·8 Ma (2SD), whereas its zircon U–Pb age (M. A. Hamilton, D. G. Pearson & R. N. Thompson, unpublished data) is 55·89 ± 0·15 Ma (2SD). It therefore remains uncertain whether the Spitzkoppe dyke swarm was emplaced at ~125 Ma or a few million years earlier, such as the ~132 Ma date for similar mafic dykes in the Brandberg, Huab and Horingbaai areas to the north and the nearby Erongo complex (Wigand *et al.*, 2003). The weight of evidence regionally clearly favours the 132 Ma date.

PETROGRAPHY AND PICRITE MINERALOGY

The thick picrite dykes are coarse and gabbroic. Their abundant olivines enclose only small chromites, whereas the plagioclase and clinopyroxene are intergrown. Small orthopyroxenes are scattered around the margins of the olivines and there are traces of interstitial biotite. Basalt dykes are finer grained and either aphyric (intergrown olivine, plagioclase and clinopyroxene) or contain small olivine phenocrysts. Intermediate dykes (5·4–1·7 wt % MgO) have sparse plagioclase phenocrysts; some euhedral and others rounded. Early pigeonite has been identified optically in VB8. The groundmass becomes progressively finer grained until it is devitrified glass in the felsic dykes. The dominant phenocrysts in the felsic dykes are quartz and turbid sericitized feldspar. Clinopyroxene phenocrysts are extremely scarce (two out of 32 samples). The picrites are almost devoid of visible low-temperature alteration but reaction of ferromagnesian minerals to chlorite ranges from ~10% to >80% in some of the less Mg-rich dykes. Our geochemical tests of the effects of this alteration are described below.

Picrite mineral compositions

Samples from two thick picrite dykes were studied by electron probe microanalysis at Manchester University [see Thompson *et al.* (2005) for method].

Olivine

Representative olivine analyses are given in Table 1. Figure 2 shows individual microprobe analyses as functions of the Mg-number of the host dyke. Rock Mg-number was calculated with 10% of total Fe as Fe^{3+} (Thompson & Gibson, 2000). Two values of K_d for the distribution of Fe^{2+} and Mg between olivine and melt are plotted: 0·30 is appropriate for equilibria between picrites and their olivines at 1 atm, whereas 0·31 applies at 0·5 GPa pressure (Ulmer, 1989). Garcia *et al.* (1995) and Garcia (1996) showed how some Hawaiian basalts and picrites from Mauna Loa and Mauna Kea are in equilibrium with their olivines, whereas others are best explained as cumulates because their olivines plot to the right of the equilibrium K_d (i.e. the bulk composition is more magnesian than would be appropriate to precipitate the olivines it contains). Using this reasoning, the olivine phenocrysts in both VB18 and 32 are clearly accumulative. The Spitzkoppe picrites therefore appear to be suspensions of olivine phenocrysts in basaltic liquids, rather than originally picritic melts. Olivines from the nearby (~100 km to the north) Horingbaai suite are also plotted in Fig. 2 for comparison (Thompson *et al.*, 2001). An obvious difference between the two suites is the lack of very magnesian olivine macrocrysts in the two Spitzkoppe picrites studied. Of course, the possibility of some post-crystallization re-equilibration of these olivines in the thick dykes cannot be ruled out but, if this has not happened, then the VB32 olivines must have been precipitated from a melt with Mg-number ~60 and the VB18 olivines from an even more Fe-rich melt.

Chromite

Euhedral chromites up to a few millimetres in size occur within the olivines in both picrites. Representative analyses are given in Table 1. Cr_2O_3 varies between about 6 and 26 wt %, and Al_2O_3 between 2·7 and 6·0 wt % in both samples but a few points show Al_2O_3 values up to 15 wt %.

Clinopyroxene

This phase is clearly late-crystallizing in the picrites as it tends towards large poikilocrysts, enclosing both olivines and plagioclases. Typical analyses are given in Table 1.

Table 1: Representative electron microprobe mineral analyses in Spitzkoppe picrite dykes

Sample	Location of analysis	SiO_2	TiO_2	Al_2O_3	Cr_2O_3	FeO	MnO	MgO	NiO	CaO	Na_2O	K_2O	Total
Olivines													
VB32	Large phenocryst core	40·24	n.m.	n.m.	0·05	15·95	0·23	44·38	0·32	0·24	n.m.	n.m.	101·41
VB32	Small phenocryst, rim	39·34	n.m.	n.m.	0·01	20·04	0·30	40·88	0·26	0·11	n.m.	n.m.	100·92
VB18	Small phenocryst core	38·29	n.m.	n.m.	0·04	20·93	0·32	39·68	0·21	0·18	n.m.	n.m.	99·65
VB18	Small phenocryst core	37·18	n.m.	n.m.	0·01	25·63	0·37	36·58	0·20	0·21	n.m.	n.m.	100·17
VB18	Small phenocryst core	37·70	n.m.	n.m.	0·01	25·41	0·35	36·28	0·22	0·14	n.m.	n.m.	100·09
Spinels													
VB32	Incl. in ol phenocryst core	0·02	0·89	6·22	25·40	58·44	0·39	3·77	0·26	n.m.	n.m.	n.m.	95·38
VB32	Incl. in ol phenocryst core	0·01	0·24	12·40	17·31	60·16	0·33	4·70	0·31	n.m.	n.m.	n.m.	95·46
VB32	Incl. in ol phenocryst core	0·01	3·67	2·89	6·01	79·22	0·27	1·92	0·37	n.m.	n.m.	n.m.	94·35
VB18	Incl. in ol phenocryst core	0·02	0·19	10·50	26·01	54·95	0·34	3·60	0·16	n.m.	n.m.	n.m.	95·76
VB18	Incl. in ol phenocryst core	0·02	0·23	15·01	23·75	51·89	0·34	4·84	0·17	n.m.	n.m.	n.m.	96·25
VB18	Incl. in ol phenocryst core	0·03	8·26	2·66	6·71	75·23	0·38	2·06	0·22	n.m.	n.m.	n.m.	95·54
Ilmenite													
VB32	Incl. in ol phenocryst core	0·01	47·38	0·04	1·17	42·72	0·53	6·35	0·08	n.m.	n.m.	n.m.	98·27
Clinopyroxenes													
VB18	Very large poikilocryst	51·22	0·35	4·15	1·28	5·50	0·16	16·83	0·06	19·84	0·25	n.m.	99·64
VB18	Very large poikilocryst	50·74	0·97	2·79	0·17	9·92	0·25	16·34	0·05	17·86	0·37	n.m.	99·46
VB18	Very large poikilocryst	52·14	0·35	3·75	1·14	5·28	0·12	16·41	0·05	21·24	0·25	n.m.	100·74
VB32	Very large poikilocryst	51·61	0·34	2·75	0·86	5·57	0·15	17·02	0·05	20·83	0·31	n.m.	99·47
Orthopyroxene													
VB18	Large poikilocryst	54·08	0·58	1·03	0·02	16·34	0·41	26·06	0·05	1·87	0·05	n.m.	100·50
VB32	Large poikilocryst	55·12	0·30	0·58	0·00	14·20	0·35	28·47	0·10	1·10	0·03	n.m.	100·24
Biotite													
VB32	Very small interstitial crystal	39·61	4·75	12·19	0·01	10·07	0·02	19·23	0·18	0·00	0·23	9·12	95·41

All Fe measured as FeO. n.m., not measured; incl., inclusion; ol, olivine. [See Thompson *et al.* (2005) for analytical methods.]

Orthopyroxene

This mineral forms small subhedra, mostly close to the margins of olivines, and larger poikilitic crystals. Two analyses are given in Table 1.

Biotite

Small interstitial crystals of biotite are visible in trace quantities within both picrites, especially VB32, and an analysis is given in Table 1. Without analysis for fluorine, it cannot be certain that this biotite is necessarily hydrous and therefore indicative of a wet magma (see below).

Alkali feldspar

Element maps show that alkali feldspar also occurs interstitially in VB32.

GEOCHEMISTRY

Methods

Analytical methods are described in Electronic Appendix A, available for downloading at http://www.petrology.oxfordjournals.org.

Results

Element and oxide variation

The analyses (Table 2) show wide ranges of MgO (20·1–0·1 wt %) and SiO_2 (46·0–68·2 wt %). Additionally, five acid dykes from around the Gross Spitzkoppe granite stock, analysed by Frindt *et al.* (2004*a*) are plotted in the following diagrams where appropriate. Samples with >12 wt % MgO are called picrites in this paper (Le Bas, 2000). On a plot of ($Na_2O + K_2O$) vs SiO_2 (TAS; Le Maitre, 2002) the new analyses plot along the same trend as published data for the HB–O swarm dykes (Trumbull *et al.*, 2004*a*, fig. 3), through the fields basalt, andesite, dacite and rhyolite but adjacent to the boundary with the basalt–trachyte suite.

A plot of selected oxides (wt %) and trace elements (ppm) vs MgO (Fig. 3) in the Spitzkoppe picrite–rhyolite dykes shows that both Cr and Ni fall progressively with MgO. Although the variations of SiO_2, Cr and Ni with MgO are smooth curves in Fig. 3, the behaviour of the other major oxides and Sc in this diagram is more complex. Trend lines have been drawn (by eye) to

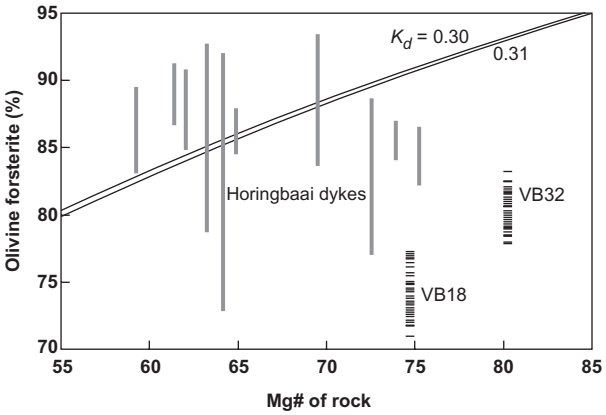

Fig. 2. Mg-number of olivine phenocrysts in two Spitzkoppe picrites (VB18 and 32) vs Mg-number of the rocks containing them. Individual olivine analyses are shown as short horizontal bars. Similar data from contemporaneous Horingbaai dykes in the Brandberg–Huab area (Fig. 1, inset) are summarized as grey vertical bars, for comparison (Thompson *et al.*, 2001). Given K_d values of 0·30–0·31 for Fe^{2+}–Mg partitioning at equilibrium between basic melts and olivine (Ulmer, 1989), the phenocrysts in VB18 and 32 must be accumulative (see text).

illustrate qualitatively the extent to which each plot is described by an inflected trend, such as may occur during fractional crystallization of melts by the addition of a new mineral to the separating phases. Such inflected trend-lines describe the behaviour of CaO, Al_2O_3 and Sc well (Fig. 3). In the Fe_2O_3, TiO_2 and P_2O_5 plots there is a handful of points lying far above the trends fitting the other data. Thin sections of the samples showing these relatively high Fe_2O_3, TiO_2 and P_2O_5 values have visible populations of titanomagnetite and apatite microphenocrysts that may be accumulative.

The trend inflections for Fe_2O_3 and TiO_2 in Fig. 3 correspond approximately to the appearance of titanomagnetite in thin sections, as MgO falls to ~3·5 wt %. Likewise, the inflection of the P_2O_5 trend at ~3·0 wt % MgO marks the appearance of apatite microphenocrysts. The inflection at ~6·5 wt % MgO in the Al_2O_3 plot corresponds to the appearance of plagioclase as a phenocryst. In contrast, the inflections at ~9·0 wt % MgO in the CaO and Sc trends do not correspond to the first appearance as phenocrysts of any mineral, such as Ca-rich clinopyroxene, that might remove these two elements together from a melt. The only visible phenocryst in dykes with MgO contents on both sides of this inflection is olivine (sometimes with chromite inclusions), a mineral poor in both Ca and Sc. Clinopyroxene is conspicuously absent as phenocrysts in the Spitzkoppe basic and intermediate dykes.

The two fields drawn on the TiO_2–MgO plot (Fig. 3) encompass >1000 analyses of lavas and hypabyssal intrusions from throughout the Etendeka Igneous Province (Marsh *et al.*, 2001), showing how they divide into low-Ti and high-Ti magmatic suites. Between these fields a group of 12 analyses has been omitted for clarity. These are the Tafelkop basalts of Marsh *et al.* (2001), known by others as 'LTZ.H' (Ewart *et al.*, 1998*a*) or ferropicrites–basalts (Gibson *et al.*, 2000). It should be noted that, although the two fields in Fig. 3 and their subdivisions were described as mafic by Marsh *et al.* (2001), and most of the subdivisions are formally named 'basalts', the analyses defining the two fields include compositions with MgO as low as 3 wt %. The Spitzkoppe dykes clearly form part of the Etendeka low-Ti suite.

The array of patterns produced by rare earth element (REE) variation in the Spitzkoppe dykes (Fig. 4) is qualitatively concordant with the data on Fig. 3. The progressive increase in all the REE, except Eu, from picrites to rhyolites is consistent with a fractional crystallization process creating this magma suite. Apart from aphyric basalts VB20 (no Eu anomaly) and VB24 (small positive Eu anomaly), all the samples have negative Eu anomalies. These are approximately constant throughout dykes that lack plagioclase phenocrysts and increase in plagioclase-phyric intermediate and acid dykes (see Fig. 14 below).

Isotopes

The radiogenic isotopic ratios of the Spitzkoppe dykes show large variations (Tables 3 and 4) and these rule out the possibility that their range of elemental compositions could be due to closed-system fractional crystallization of a basic magma. The isotopic ratios are corrected to an emplacement age of 132 Ma, for reasons explained above.

Tests for effects of low-temperature alteration and very small-scale sample isotopic heterogeneity. The isotope data for dykes in Table 3 can be used to test the effects of low-temperature hydrothermal alteration because samples analysed at McMaster were all first leached in acid whereas those analysed at Durham were not. Eight dyke samples were analysed for Pb isotopes in both laboratories. Excluding the rhyolite sample VB30, the R^2 value for the regression between the two sets of $^{206}Pb/^{204}Pb$ data (the ratio with the largest range of values) is 0·999. Rhyolite VB30 falls slightly off this regression (R^2 drops to 0·994) and this may be due to the turbid hydrothermal alteration of its predominant alkali feldspar.

There are small significant differences between $^{87}Sr/^{86}Sr$ for the McMaster and Durham analyses of picrites VB18 and 32. Although these could be alteration related, they are not both in the same direction. There is also a significant difference between the results of the two laboratories for $^{143}Nd/^{144}Nd$ in VB18, discussed in detail in Electronic Appendix A. It is generally accepted that the latter are unlikely to be related to the slight alteration of this sample. These data suggest small-scale isotopic variability within the picrites—as might be expected from the crustal assimilation model to be developed below. Although lava samples are usually isotopically homogeneous at the hand-specimen level, it is becoming clear that this

Table 2: Whole-rock analyses of dykes from the Spitzkoppe swarm and Damara Belt crustal rock-types

	Dykes																	
Sample:	VB32	VB11	VB3	VB19	'Model' VB19[1]	VB18	VB25	VB1	VB26	VB4	VB5	VB24	VB20	VB14	VB6	VB8	VB23	VB16
SiO_2	46·32	45·95	47·89	46·64	48·59	46·94	46·30	47·69	46·67	46·47	48·25	49·01	47·99	50·39	48·56	49·45	51·72	52·89
TiO_2	0·54	0·54	0·83	0·91	0·84	0·62	0·76	1·04	1·03	1·09	1·06	1·04	1·34	1·07	1·40	1·14	1·48	1·49
Al_2O_3	11·26	11·54	11·63	12·97	13·02	13·46	13·52	14·02	13·47	14·89	14·88	15·27	14·32	16·02	15·94	15·07	14·97	15·00
Fe_2O_3*	10·93	11·08	11·75	11·39	11·15	10·85	11·01	11·30	11·87	11·65	11·20	11·92	12·22	11·09	12·08	10·27	11·24	11·69
MnO	0·14	0·16	0·19	0·17	0·00	0·16	0·17	0·19	0·19	0·17	0·16	0·19	0·20	0·18	0·19	0·14	0·17	0·20
MgO	20·14	19·30	15·03	14·68	14·83	14·56	12·84	11·40	11·09	10·27	9·25	7·74	7·24	6·90	6·23	5·43	5·32	5·02
CaO	8·76	8·88	9·51	9·81	10·20	10·78	10·36	10·85	11·40	10·87	10·03	11·11	11·04	10·11	9·48	8·79	9·06	8·94
Na_2O	1·40	1·35	1·42	1·72	1·18	1·54	1·61	1·77	1·80	1·80	2·16	2·21	2·19	1·88	2·56	2·30	2·42	2·14
K_2O	0·27	0·29	0·29	0·41	0·12	0·29	0·43	0·41	0·40	0·52	0·83	0·49	0·53	1·51	1·25	1·74	1·71	1·77
P_2O_5	0·05	0·05	0·07	0·11	0·07	0·06	0·11	0·13	0·13	0·18	0·13	0·08	0·14	0·12	0·26	0·17	0·20	0·20
SO_3	0·08	0·06	n.d.	0·09	0·00	0·06	0·07	n.d.	n.d.	0·08	0·09	n.d.	n.d.	n.d.	n.d.	0·26	n.d.	n.d.
Total	100·27	99·22	100·00	99·33	100·00	99·33	98·44	100·81	99·87	98·71	99·20	100·22	99·46	100·14	100·23	99·58	99·74	100·39
LOI	0·38	gain	1·39	0·42		0·02	1·27	2·01	1·82	0·74	1·16	1·18	2·25	0·85	2·27	4·82	1·45	1·05
Mg-no.	80·22	79·30	73·78	73·92		74·70	71·97	68·94	67·28	65·98	64·51	58·82	56·60	57·78	53·14	53·80	51·01	48·58
Ba	49	57	145	139		75	158	194	188	240	312	157	169	399	587	462	569	565
Cr	1892	2051	1794	1557		1628	1296	896	852	603	508	263	135	99	47	22	64	38
Hf	1·09	1·13	1·97	1·85		1·28	1·62	2·50	2·10	2·53	3·44	2·20	2·72	3·58	4·53	4·86	5·90	5·15
Nb	2·9	3·0	4·1	5·8		3·9	4·5	8·7	5·6	7·5	7·6	3·9	7·0	8·0	24·2	10·7	13·6	14·2
Ni	986	959	585	609		583	475	314	343	279	304	31	64	149	48	30	45	16
Pb	1·41	1·53	2·32	2·05		1·59	2·17	2·38	2·31	2·32	5·10	3·08	3·20	4·29	6·08	10·32	11·04	20·14
Rb	11·7	12·5	22·7	12·6		9·4	20·3	21·9	13·9	18·2	30·1	12·5	17·4	82	37	61	59	89
Sc	31	33	33	36		40	37	37	36	37	32	34	35	29	32	24	26	29
Sr	69	75	143	174		102	170	214	212	268	234	268	275	216	315	325	275	260
Ta	0·25	0·26	0·26	0·40		0·30	0·29	0·51	0·33	0·45	0·44	0·24	0·43	0·49	1·36	0·61	0·77	0·81
Th	0·93	1·02	1·38	1·13		1·05	1·51	1·06	0·94	0·78	2·54	1·34	2·30	4·06	4·63	7·77	7·89	6·79
U	0·37	0·40	0·19	0·30		0·34	0·26	0·22	0·19	0·17	0·34	0·22	0·43	0·59	0·71	1·03	0·96	0·79
V	226	222	278	277		255	265	263	291	277	285	242	363	258	208	164	190	193
Y	17	18	21	23		22	22	26	23	25	29	22	25	29	37	35	40	41
Zr	40	41	74	67		45	57	96	77	98	138	77	100	140	181	188	233	198
La	10·2	45·9	7·8	10·2		15·9	28·7	54·4	27·4	84·5	81·0	3·7	90·8	17·8	31·4	32·1	244·4	4·3
Ce	22·3	94·7	16·7	22·8		33·3	57·1	108·6	56·1	169·9	162·6	8·0	185·5	37·0	63·8	65·3	476·1	9·4
Pr	3·16	12·33	2·36	3·37		4·50	7·40	14·07	7·43	22·38	21·49	1·15	24·92	4·98	8·40	8·59	61·29	1·38
Nd	14·2	47·6	10·6	15·3		19·1	29·7	56·0	30·1	89·6	86·6	5·3	101·4	20·5	34·2	34·8	229·7	6·4
Sm	3·46	9·55	2·69	3·69		4·32	6·04	10·75	6·22	16·75	16·34	1·60	19·70	4·59	7·13	7·27	40·03	1·91
Eu	1·08	1·39	0·86	1·19		1·27	1·73	2·56	1·53	4·13	4·02	0·56	4·45	1·26	1·78	1·82	4·41	0·67
Gd	4·11	8·76	3·29	4·25		4·84	6·23	10·25	6·26	15·37	14·81	2·38	18·51	4·89	7·31	7·55	32·88	2·79
Tb	0·68	1·32	0·57	0·69		0·81	1·02	1·59	0·98	2·28	2·19	0·43	2·81	0·82	1·17	1·21	5·10	0·53
Dy	4·24	7·54	3·40	4·20		4·87	6·22	9·24	5·84	12·85	12·48	2·81	15·84	4·91	6·96	7·10	28·58	3·43
Ho	0·88	1·48	0·71	0·86		1·00	1·29	1·86	1·19	2·53	2·47	0·61	3·13	1·01	1·43	1·43	5·49	0·74
Er	2·45	4·05	1·95	2·35		2·73	3·61	5·05	3·24	6·76	6·57	1·74	8·48	2·70	3·88	3·88	14·63	2·15
Tm	0·38	0·62	0·30	0·37		0·42	0·57	0·78	0·50	1·03	0·99	0·27	1·29	0·42	0·60	0·59	2·27	0·34
Yb	2·45	3·83	1·85	2·34		2·65	3·62	4·96	3·19	6·51	6·25	1·74	8·06	2·66	3·76	3·69	14·21	2·15
Lu	0·39	0·61	0·30	0·39		0·42	0·59	0·80	0·51	1·04	1·01	0·29	1·28	0·43	0·61	0·58	2·21	0·35

(continued)

Table 2: Continued

	Dykes												Damara Belt crustal rock-types					
Sample	VB15	VB29	VB7	VB21	VB10	VB22	VB9	VB2	VB13	VB30	VB17	VB28	VB12	VB37	VB38	VB39	VB41	VB42
SiO_2	51·97	53·00	49·94	53·55	47·69	52·79	47·91	61·74	56·99	65·82	67·20	68·16	71·95	66·25	73·10	76·75	57·68	75·96
TiO_2	1·40	1·49	1·88	1·77	2·82	1·94	2·94	0·96	2·52	0·50	0·47	0·47	0·34	0·00	0·23	0·03	0·95	0·84
Al_2O_3	15·10	14·48	14·54	13·76	13·69	13·66	13·58	13·71	13·70	12·42	12·95	12·99	14·42	18·57	13·83	14·01	17·26	10·15
Fe_2O_3*	11·31	11·14	12·14	11·79	14·20	12·69	14·19	7·15	11·86	7·30	6·58	6·65	1·96	0·00	1·59	0·42	8·39	5·08
MnO	0·17	0·18	0·19	0·16	0·22	0·18	0·22	0·10	0·17	0·12	0·15	0·12	0·03	0·00	0·05	0·08	0·09	0·07
MgO	4·88	4·63	4·49	3·43	3·30	3·29	3·16	2·96	1·69	0·19	0·12	0·05	0·32	0·00	0·26	0·06	4·29	2·22
CaO	8·55	8·36	7·97	7·66	6·64	7·40	6·61	4·20	4·83	2·22	2·44	2·16	0·95	0·07	1·37	0·34	1·47	0·80
Na_2O	2·37	2·23	2·54	2·42	2·89	2·34	2·88	2·54	2·17	2·73	2·92	2·85	3·11	3·18	5·32	3·66	1·44	1·05
K_2O	1·80	1·76	2·10	2·53	2·73	2·62	2·93	3·83	4·07	5·58	4·63	5·18	6·28	11·05	2·30	4·31	3·36	2·37
P_2O_5	0·20	0·20	0·48	0·26	0·98	0·27	0·97	0·20	1·17	0·09	0·09	0·08	0·13	0·40	0·10	0·16	0·24	0·13
SO_3	0·10	n.d.	n.d.	n.d.	n.d.	n.d.	n.d.	n.d.	n.d.	0·10	n.d.	n.d.	0·05	n.d.	n.d.	0·05	n.d.	n.d.
Total	99·23	99·52	99·43	99·97	99·68	100·21	99·30	98·07	99·82	99·03	99·02	99·71	99·90	99·69	98·50	100·56	100·00	100·21
LOI	1·39	2·05	3·15	2·62	4·51	3·05	3·91	0·59	0·64	1·96	1·46	1·01	0·36	0·17	0·34	0·69	4·83	1·54
Mg-no.	48·71	47·79	44·88	39·01	33·86	36·30	32·89	47·70	23·86	5·31	3·80	1·61						
Ba	583	563	874	503	1384	673	1513	640	2109	261	433	348	498	326	776	41	573	653
Cr	40	41	26	9	4	10	7	61	3	3	2	1	3	0	3	0	162	56
Hf	5·82	5·65	7·86	4·04	11·23	7·89	11·84	6·59	13·09	26·15	20·14	15·58	2·02	0·02	4·53	0·92	4·79	4·54
Nb	14·0	15·3	39·8	8·9	63·3	18·0	66·4	17·5	57·7	137	168	173	25·7	0·3	44·7	82·9	16·4	12·5
Ni	17	20	12	7	15	9	17	30	2	4	1	0	1	0	1	0	65	28
Pb	12·77	13·18	12·29	9·84	14·79	16·21	14·92	24·64	23·09	165·83	47·08	25·19	43·77	32·22	25·12	21·74	9·08	12·53
Rb	66	75	71	71	79	100	84	175	141	302	310	344	310·0	1028·8	271·4	355·9	157·8	105·9
Sc	29	28	29	15	22	25	22	18	21	8	11	10	5	0	3	1	22	11
Sr	273	253	338	219	423	286	432	188	458	42	35	36	87	33	180	17	78	37
Ta	0·79	0·87	2·03	0·52	3·00	1·02	3·13	1·06	2·76	7·54	7·86	8·09	1·55	0·10	5·95	14·86	1·28	0·99
Th	6·74	7·47	7·97	9·99	8·35	12·88	8·94	19·47	13·04	58·90	34·53	35·35	50·82	0·03	18·47	0·85	13·67	9·83
U	0·83	0·87	1·37	0·97	1·56	1·87	1·70	3·37	2·19	7·02	5·72	5·51	5·33	0·85	6·06	2·38	4·70	3·13
V	192	182	220	79	252	147	252	137	132	2	2	1	12	0	12	0	232	83
Y	41	43	54	38	73	52	74	44	91	183	159	155	25·1	0·2	27·4	3·5	35·3	26·1
Zr	227	218	328	156	485	308	508	251	531	1058	711	538	62	1	157	12	176	159
La	6·9	11·3	33·1	44·0	32·4	7·6	7·6	9·1	254·5	34·9	236·3	3·40	87·82	0·30	42·81	1·14	39·27	40·86
Ce	15·5	24·9	66·5	90·3	66·1	17·4	16·5	20·9	493·0	70·7	512·3	7·51	181·46	0·47	75·89	2·10	80·00	81·74
Pr	2·29	3·62	8·80	11·97	8·53	2·57	2·36	3·03	63·41	9·29	59·59	1·11	22·28	0·05	8·47	0·22	10·42	10·48
Nd	10·7	16·1	36·4	48·1	35·6	12·2	10·5	14·2	237·1	37·7	231·6	5·19	77·75	0·19	28·95	0·73	40·91	40·66
Sm	2·82	3·97	7·42	9·90	7·38	3·21	2·66	3·52	41·06	7·71	42·08	1·52	13·33	0·05	5·21	0·26	8·05	7·77
Eu	0·94	1·37	1·55	2·04	1·78	1·23	0·85	1·10	4·27	1·82	1·70	0·52	0·92	0·07	0·93	0·09	1·54	1·34
Gd	3·64	4·55	7·16	9·62	7·22	3·65	3·33	3·92	33·21	7·71	37·02	2·22	9·19	0·04	4·62	0·33	7·02	6·49
Tb	0·62	0·74	1·12	1·51	1·15	0·63	0·58	0·65	5·04	1·23	5·62	0·41	1·22	0·01	0·77	0·08	1·08	0·91
Dy	3·86	4·41	6·46	8·82	6·74	3·83	3·63	3·90	27·84	7·31	32·15	2·67	5·58	0·05	4·44	0·53	6·04	4·74
Ho	0·82	0·89	1·32	1·80	1·40	0·80	0·76	0·80	5·24	1·47	6·54	0·58	0·89	0·01	0·89	0·10	1·19	0·91
Er	2·28	2·45	3·57	4·92	3·79	2·15	2·16	2·21	13·52	3·99	17·58	1·65	1·90	0·02	2·44	0·34	3·34	2·36
Tm	0·36	0·38	0·56	0·76	0·59	0·34	0·34	0·34	2·02	0·60	2·72	0·26	0·24	0·00	0·39	0·08	0·55	0·37
Yb	2·25	2·36	3·54	4·78	3·71	2·14	2·18	2·19	12·25	3·79	17·14	1·66	1·32	0·02	2·57	0·69	3·56	2·38
Lu	0·36	0·38	0·58	0·78	0·60	0·35	0·34	0·34	1·82	0·60	2·68	0·27	0·19	0·00	0·40	0·11	0·57	0·39

*Total Fe recorded as Fe_2O_3.
[1]See text.
n.d., not detected. Dyke analyses are in order of descending MgO content. Major elements analysed by XRF (see text for methods). Trace elements analysed by XRF and ICP-MS (see text for methods). Localities of dykes and Damara granite VB12 are shown in Fig. 1. Other Damara Belt rock-types: VB37, 38 and 39 are pegmatite K-feldspar, granite and aplite, respectively (21°19·132′S, 14°43·210′E); VB41 is phyllite (20°51·084′S, 14°7·857′E); VB42 is mica schist (20°43·410′S, 14°18·563′E). World Geodetic System revision WGS84 datum.

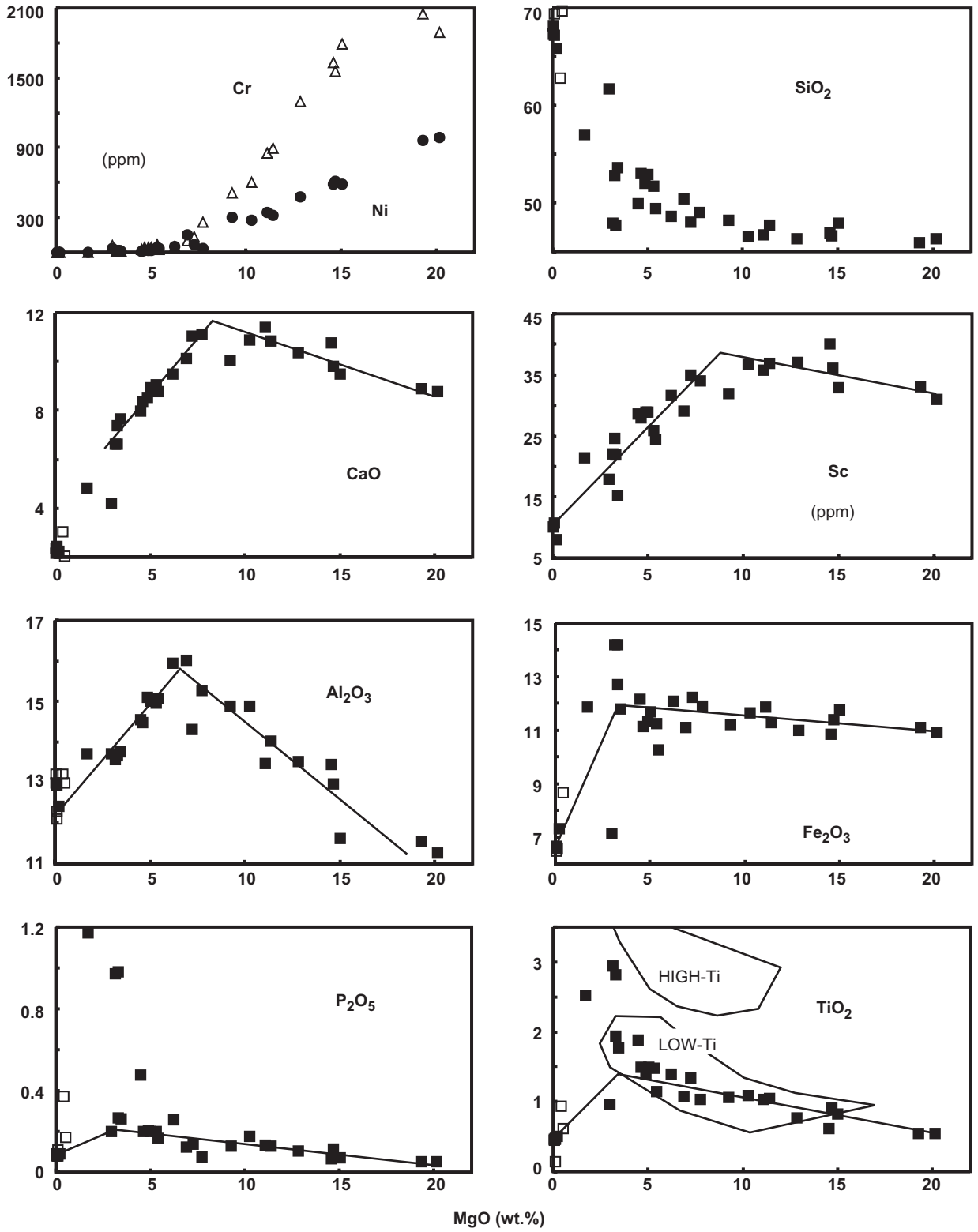

Fig. 3. Variations of selected oxides and Sc in the Spitzkoppe dykes as functions of MgO. ■, Spitzkoppe picrite–rhyolite dykes (Table 2); □, Spitzkoppe acid dykes (Frindt *et al*, 2004*a*). Separate symbols (● and △) are used for all the dykes in the Cr–Ni plot, for clarity. Trend lines are drawn by eye. High- and low-Ti Etendeka lava fields from Marsh *et al.* (2001).

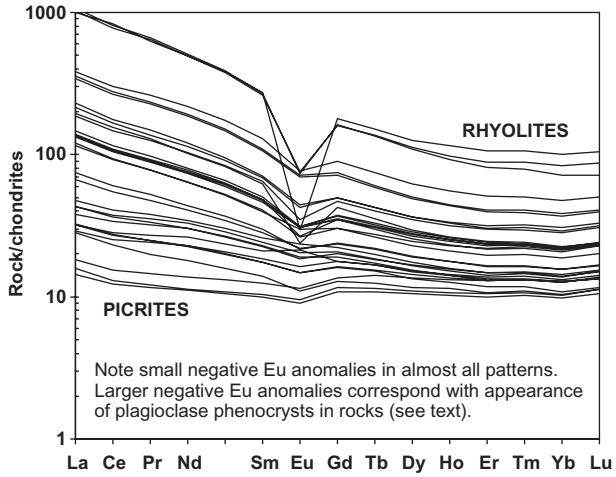

Fig. 4. Chondrite-normalized rare earth elements in the Spitzkoppe dyke samples.

homogeneity is illusory, in that glass inclusions within the olivine phenocrysts of some crustally contaminated continental picrites are extremely heterogeneous in both elements and isotopes (e.g. Yaxley *et al.*, 2004; Harlou *et al.*, 2006). Such inhomogeneity should logically eventually be expected to occur between aliquots from a powdered individual olivine-phyric hand specimen, and samples VB18 and 32 appear confirm this point. Clearly, this matter requires more research.

Sr, Nd and Hf isotopes. On a plot of $^{87}Sr/^{86}Sr$ vs εNd (Fig. 5) the picrite–intermediate dykes form a steep continuous array. The picrites have εNd values just above and just below zero, within the field of ocean island basalts (OIB), whereas εNd values for the intermediate and rhyolite dykes fall in the range from −5 to −10. New analyses of crustal rocks comprise: Damara granite VB12, which crops out within the dyke swarm [Frindt *et al.* (2004*b*) analysed another Damara granite sample, SF17, ~1·5 km SE of VB12, Fig. 1]; Damara granite (VB38) and associated aplite (VB39) and pegmatite alkali feldspar (VB37), which crop in the Horingbaai mafic dyke swarm, south of the Brandberg intrusive complex (Thompson *et al.*, 2001); Damara phyllite (VB41) and metasedimentary schist (VB42) between the Brandberg and Huab areas (Fig. 1). Some of these crustal rocks tend to enlarge the Sr–Nd isotopic fields for Damara granites and metasediments plotted by Frindt *et al.* (2004*b*). A mixing curve between picrite dyke VB32 (highest εNd) and the local Damara granite (VB12/SF17) does not pass through the dyke data. The field for pre-Damara basement in the Spitzkoppe area is speculative and follows the suggestion of Frindt *et al.* (2004*b*) and others that the Damara belt may be underlain by the same Archaean–Proterozoic gneisses as form the Congo–Angola craton in Kaokoland, NW Namibia (Seth *et al.*, 1998). If this is so, such a deep-crust basement would form a suitable crustal end-member for a mixing curve passing through the picrite and basalt dyke data in Fig. 5. Tangible isotopic evidence for a deep-crust basement of this composition is provided by rhyolites from the Cretaceous Paresis sub-volcanic complex, NE of Spitzkoppe (Fig. 1, inset), which have Sr–Nd isotopic ratios (Fig. 5) very similar to those of the Kaokoland gneisses (Mingram *et al.*, 2000). In this paper we use Paresis rhyolite PA19 (Mingram *et al.*, 2000) as a geochemical proxy for partial melts of acid–intermediate lower crust in the Damara region. This is obviously less satisfactory than having lower crust samples available.

Table 3 and Fig. 6 show the first Hf-isotope data published for both Etendeka igneous rocks and Damara belt crustal rocks. The dyke data show covariation of εNd and εHf, such that the picrites and basalts fall in the OIB field whereas the intermediate and rhyolite dykes have similar Nd–Hf isotope ratios to the local Damara belt exposed crust. The MgO content of each Spitzkoppe dyke is marked in Fig. 6, so that the overall correlation between MgO and Nd–Hf isotopic ratios in the dykes can be seen.

Pb isotopes. When it became clear that Pb isotope variation in the Spitzkoppe dyke swarm is complex, we analysed sample sets at both Durham and McMaster, so as to maximize the data and also to provide interlaboratory cross-checks (Table 3). At first sight, Pb isotopes in the Spitzkoppe dykes (Table 3) behave in much the same way as their Sr–Nd–Hf isotopes, in that the picrites and Mg-rich basalts form a linear array, with a good correlation between Pb isotopes and MgO in the 20–9 wt % range (Fig. 7). However, the rhyolite dyke VB30, and also dyke SF11d of Frindt *et al.* (2004*b*) show a major difference. Instead of continuing the trend of the mafic dykes to lower $^{206}Pb/^{204}Pb$ ratios, they have relatively high $^{206}Pb/^{204}Pb$ and $^{208}Pb/^{204}Pb$ ratios and thus, in terms of Pb isotopes, appear to be unrelated to the picrites and basalts. The Mg-poor basalts and intermediate dykes (MgO ~8–3 wt %) divide between these Pb isotopic groups; the majority have relatively low $^{206}Pb/^{204}Pb$, combined with slightly higher $^{208}Pb/^{204}Pb$ than the Mg-rich basalts (Fig. 7), but two Mg-poor basalts, VB14 and 16, cluster with the rhyolite dykes in terms of their Pb isotopes. The field for Damara S-type granites (Frindt *et al.*, 2004*b*) must be enlarged slightly to incorporate our new Pb-isotope data for these rock-types (Table 3 and Fig. 7) and the Spitzkoppe rhyolite dykes plot within the enlarged fields. They also lie close to the Gross Spitzkoppe granite field (Frindt *et al.*, 2004*b*). The field for southern Etendeka LTZ lavas and dykes incorporates data for so-called continental flood basalt (CFB)-like dykes in the nearby Brandberg area (Thompson *et al.*, 2001; Fig. 1, inset). This field has been redefined in Fig. 7 by reanalysis of key samples (Table 3). After such standardization, it becomes clear in Fig. 7 that the elongation of this field is collinear with Pb isotopic variation in the Spitzkoppe picrites and

Table 3: Sr, Nd, Hf and Pb isotopes in Spitzkoppe dykes and Damara Belt crustal rock-types

Sample	MgO (wt %)	$^{87}Sr/^{86}Sr$	$(^{87}Sr/^{86}Sr)_{132}$	$^{143}Nd/^{144}Nd$	$(^{143}Nd/^{144}Nd)_{132}$	$(\varepsilon Nd)_{132}$	$^{176}Hf/^{177}Hf$	$(^{176}Hf/^{177}Hf)_{132}$	$(\varepsilon Hf)_{132}$	$^{206}Pb/^{204}Pb$	$(^{206}Pb/^{204}Pb)_{132}$	$^{207}Pb/^{204}Pb$	$(^{207}Pb/^{204}Pb)_{132}$	$^{208}Pb/^{204}Pb$	$(^{208}Pb/^{204}Pb)_{132}$
Spitzkoppe dykes															
VB32	20·14	0·708038(58)	0·707118	0·512657(15)	0·512503	0·69	0·282944(10)	0·282857	5·91						
VB32	20·14	0·70772(3)	0·70680	0·512670(20)	0·512542	1·44				19·79	19·44	15·711	15·694	38·95	38·66
VB11	19·30	0·709138(12)	0·708234	0·512548(10)	0·512390	−1·53	0·282908(9)	0·282786	3·38	19·70	19·35	15·723	15·706	38·97	38·68
VB19	14·68	0·707228(10)	0·706835	0·512530(7)	0·512392	−1·49	0·282854(10)	0·282737	1·64	18·99	18·80	15·673	15·664	38·82	38·58
VB18	14·56	0·708033(34)	0·707530	0·512623(10)	0·512467	−0·03	0·282916(16)	0·282668	−0·79						
VB18	14·56	0·70814(3)	0·70764	0·512495(17)*	0·512376	−1·80				19·35	19·06	15·697	15·683	38·91	38·62
VB1	11·40	0·70899(4)	0·70844	0·512460(22)	0·512359	−2·12				18·59	18·47	15·658	15·652	38·59	38·55
VB26	11·09	0·70819(2)	0·70784	0·512405(15)	0·512296	−3·35									
VB4	10·27	0·707855(12)	0·707487	0·512427(8)	0·512301	−3·27	0·282686(8)	0·282564	−4·47						
VB5	9·25	0·71314(2)	0·71244	0·512219(11)	0·512120	−6·79				18·38	18·29	15·644	15·640	38·73	38·51
VB24	7·74	0·71099(3)	0·71074	0·512550(10)	0·512392	−1·49									
VB20	7·24	0·70952(3)	0·70918	0·512620(15)	0·512518	0·97									
VB14	6·90	0·715205(37)	0·713138	0·512248(12)	0·512130	−6·59									
VB6	6·23	0·71108(2)	0·71045	0·512271(17)	0·512162	−5·98				18·73	18·57	15·654	15·646	38·96	38·63
VB23	5·32	0·714904(20)	0·713743	0·512177(8)	0·512068	−7·81	0·282484(7)	0·282397	−10·38						
VB16	5·02	0·716027(10)	0·714174	0·512184(9)	0·512074	−7·68	0·282481(8)	0·282399	−10·31						
VB29	4·63	0·71652(2)	0·71491	0·512116(15)	0·511987	−9·40									
VB7	4·49	0·71122(3)	0·71008	0·512292(15)	0·512185	−5·52									
VB9	3·16	0·709824(10)	0·708770	0·512294(8)	0·512196	−5·31	0·282536(5)	0·282500	−6·74						
VB30	0·19	0·773904(20)	0·734691	0·512032(7)	0·511937	−10·37	0·282333(5)	0·282265	−15·05	19·24	19·18	15·689	15·686	39·36	39·20
Damara Belt crust															
VB12 (granite)	0·32	0·795559(29)	0·776054	0·511804(10)	0·511714	−14·72	0·282230(12)	0·282132	−19·76	18·90	18·74	15·657	15·649	39·10	38·59
VB37 (K-feldspar)	0·00	1·397599(83)	1·217119							18·46	18·42	15·634	15·632	37·88	37·88
VB38 granite)	0·26	0·738640(13)	0·730444	0·512335(9)	0·512241	−4·44	0·282599(10)	0·282501	−6·69	19·27	18·95	15·688	15·672	38·71	38·39
VB39 (aplite)	0·06	1·178757(24)	1·059865	0·512512(3)	0·512325	−2·79	0·282616(16)	0·282476	−7·59	18·89	18·75	15·665	15·658	37·97	37·95
VB41 (phyllite)	4·29	0·761506(17)	0·750454	0·512209(12)	0·512106	−7·07	0·282592(13)	0·282445	−8·68						
VB42 (schist)	2·22	0·775149(13)	0·759498	0·512245(11)	0·512145	−6·31	0·282162(12)	0·282050	−22·64	19·40	19·06	15·699	15·683	38·97	38·63

$^{87}Sr/^{86}Sr$ determined to five decimal places at McMaster (Isomass 354) and to six at Durham and OU (Neptune/Triton). Values in parentheses are ±2SE. Elemental abundances are given in Table 2.
*Average of two aliquots.

Table 4: Osmium isotopes in olivine phenocrysts of Spitzkoppe picrites

Sample	Re (ppb)	Os (ppb)	$^{187}Re/^{188}Os$	$^{187}Os/^{188}Os$	$(^{187}Os/^{188}Os)_{132}$	$(\gamma Os)_{132}$*
VB18 (ol pheno)	0·1768	1·05	0·8107	0·126041	0·124262	−1·93
VB32 (ol pheno)	0·269	0·837	1·5481	0·129656	0·126248	−0·35

*Calculated using parameters listed by Pearson *et al.* (2004).
Uncertainty in $^{187}Re/^{188}Os$ is 12·8% based on replicates of the GP13 peridotite standard (Pearson *et al.*, 2004). Uncertainty based purely on spike calibration is *c*. 1%. In-run precisions for $^{187}Os/^{188}Os$ are all better than the external precision quoted for the standard (0·25%) and are better than 0·1%. Bulk Earth $^{187}Os/^{188}Os$ taken as 0·1271. Olivine phenocrysts were separated by hand-picking. Opaque inclusions within olivine grains were accepted in separate. Re-Os analytical methods follow those given in Pearson and Woodland (2000) and Pearson and Nowell (2004).

Mg-rich basalts. The most Mg-rich Spitzkoppe picrites have $^{206}Pb/^{204}Pb$ >19·0, which is higher than values of this ratio in both Tristan da Cunha and Walvis Ridge lavas, and also in previously studied Damaraland Cretaceous picrite–basalt dykes (Thompson *et al.*, 2001; Gibson *et al.*, 2005).

Os isotopes. Osmium isotopes were determined on separated olivine phenocrysts from picrites VB18 and 32, to see whether this early crystallizing phase might have trapped oxides or sulphides before the magmas were exposed to crustal contamination. The separates were made by hand-picking, with fragments containing opaque inclusions left in the separate, rather than removed. Using an emplacement age of 132 Ma, the initial $^{187}Os/^{188}Os$ ratios of the picrite olivines (Table 4) are 0·126248 (VB32) and 0·124262 (VB18). The significance of these results will be discussed below in the section 'Focus on the picrites'.

DISCUSSION OF DYKE GEOCHEMISTRY

Open-system fractional crystallization but at what depth?

The element and oxide data summarized in Figs 3 and 4 make a strong qualitative case for fractional crystallization as the mechanism that produced the wide range of rock-types in the Spitzkoppe dykes, and the isotopic data suggest that this was an open-system (AFC) process. The composition of the parental magma is difficult to determine. All the most Mg-rich dykes in the suite are rich in olivine phenocrysts. Electron probe microanalyses of these in two of the picrites (Fig. 2) has shown that this olivine is not unusually forsteritic and therefore the high MgO of the rocks is clearly due to olivine accumulation. The most direct way to identify a likely parental composition is therefore to focus on the aphyric dyke with the highest MgO content. This is VB26 (Table 2), with 11·1% MgO.

Judging from Fig. 3, such a parental melt would have accumulated olivine phenocrysts to form the picrite suite and then evolved to the basalts, intermediate compositions and rhyolites by fractional crystallization of the following assemblages: olivine alone; ol + cpx; ol + cpx + plag; plag + cpx (ol disappears from thin sections at 5·0–5·5 wt % MgO); plag + cpx + Fe–Ti oxide; plag + cpx + oxide + apatite. The main phenocrysts observed in the rhyolites are alkali feldspar and quartz. This chemistry-based story of fractional crystallization is complicated by two items of evidence: (1) all the basalts that appear, from geochemical considerations, to have fractionated Ca-rich clinopyroxene lack phenocrysts of this mineral; (2) Sr, Nd, Hf and Pb isotope variation in the suite all imply that the fractional crystallization was open-system, with concomitant dissolution of crust in the melts.

The relative stabilities of olivine and Ca-rich clinopyroxene crystallizing from a basaltic magma are very sensitive to pressure. The most direct way to show this is by using experimental melting studies of rocks to determine the crystallization behaviour of a basic–intermediate magmatic suite as a function of pressure. After noting the 'cryptic clinopyroxene fractionation' phenomenon during 1 atm phase-equilibria studies of basic and associated lavas (Thompson, 1972), Thompson (1974) studied the Palaeocene alkali olivine basalts and hawaiites of Skye, NW Scotland, using polybaric experimental phase equilibria and showed that they had undergone extensive 'cryptic' fractionation of Ca-rich clinopyroxene (aluminous sub-calcic augite in that case) at pressures around 0·9 GPa, despite the lavas being almost devoid of augite phenocrysts in thin section. The effect of pressure on the relative stabilities of liquidus olivine and Ca-rich clinopyroxene in basaltic melts and their fractionation residua can be seen clearly in a plot of CIPW-normative ol–di–hy–ne-Q (Fig. 8). Although this projection ignores plagioclase, it is useful for illustrating the crystallization behaviour of olivine tholeiite suites such as the Spitzkoppe dykes. Parts of several cotectics are marked in Fig. 8a. They are all for the equilibrium assemblage (ol + plag + cpx + basaltic melt). The 1 atm curve was compiled by Thompson *et al.* (2001) from several sources. The 0·9 GPa curve was constructed by Thompson (1982) from the results of experimental melting *P–T* studies on olivine tholeiites, alkali basalts and hawaiites that precipitated ol, plag and cpx cotectically on their liquidi at ~0·9 GPa. The 0·2 and 0·8 GPa curves are from melting experiments on

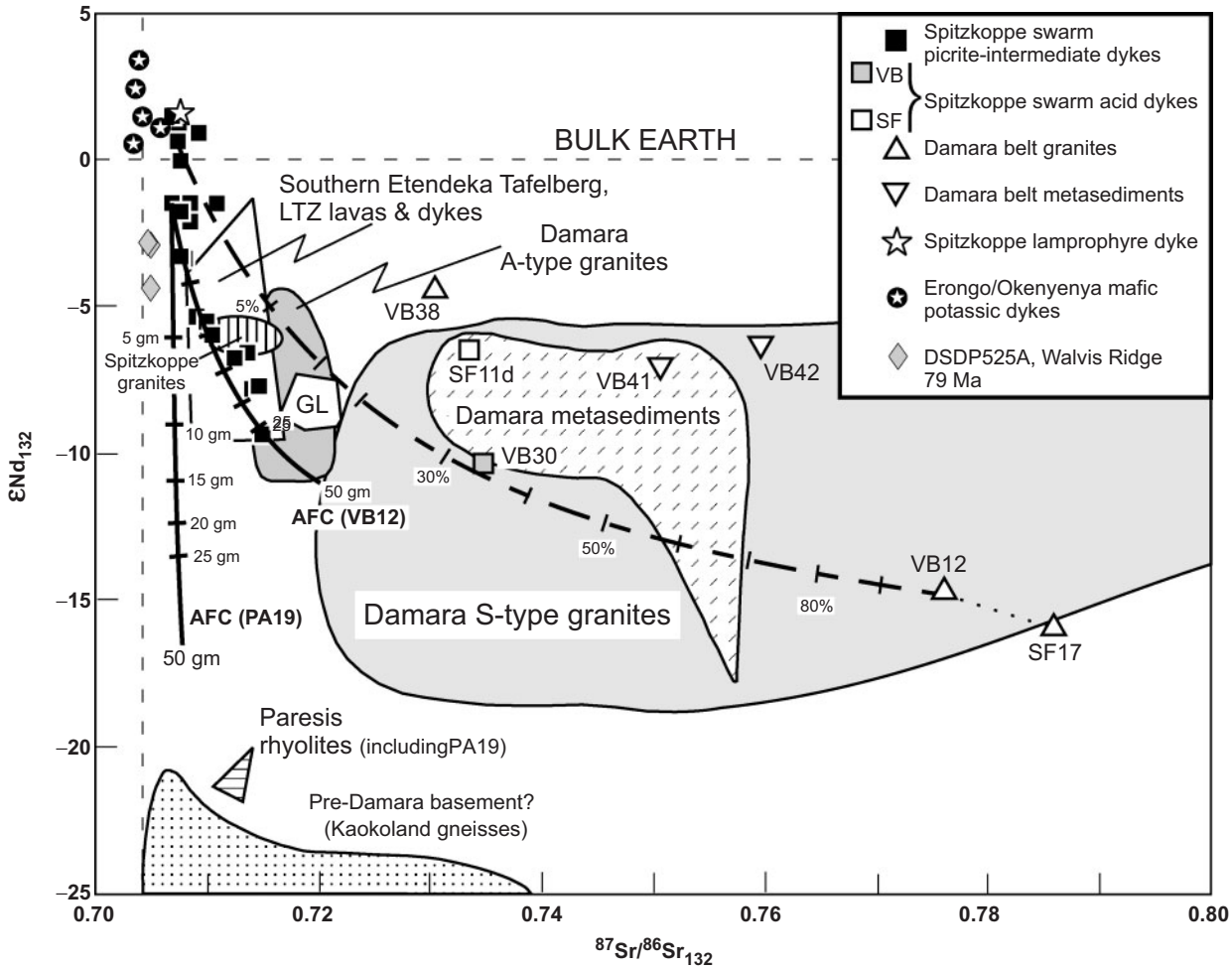

Fig. 5. Initial $^{87}Sr/^{86}Sr$ and εNd in the Spitzkoppe dykes and Damara belt granites and metasediments (at 132 Ma). VB data points from Table 2; SF data points from Frindt *et al.* (2004*a*). Fields for southern Etendeka lavas and dykes from Thompson *et al.* (2001), Goboboseb quartz latites (GL) after Ewart *et al.* (1998*b*), and Paresis rhyolites from Mingram *et al.* (2000). LTZ is 'Low Ti-Zr' (Ewart *et al.*, 1998*a*). Other fields modified after Frindt *et al.* (2004*b*). [See text for sources of the mafic potassic dykes (stars in filled circles).] Dashed line is a bulk-mixing curve between picrite VB32 and Damara granite VB12. Details are given in the text of the ticked continuous lines showing modelled AFC processes (using pMELTS) for a model picrite with MgO ~15 wt % and crustal acid rocks PA19 (Paresis rhyolite; Mingram *et al.*, 2000) and VB12 (Table 2). The model adds 1 g of crust per increment to 100 g of initial picrite and then calculates the outcome isenthalpically.

mid-ocean ridge basalt (MORB) by Grove *et al.* (1992), analysing progressive residual liquids. The 0·7 GPa curve is for experimental fractional crystallization of a tholeiite (Villiger *et al.*, 2007). A single point, marked M in Fig. 8a, is available for a Columbia River Plateau basalt (Martindale, from Helz, 1980) that shows experimental cotectic liquidus precipitation of ol + plag + cpx at 0·35 GPa, a mid-crust pressure.

All of these cotectics show consistent migration away from the Cpx apex of Fig. 8a with rising pressure. This means that a fractionating olivine tholeiite magmatic system could undergo cotectic separation of olivine and clinopyroxene in the deep crust, but any remaining clinopyroxene phenocrysts might redissolve during the subsequent uprise of the melts, so that chemical study of the suite would indicate 'cryptic' clinopyroxene fractionation. Thompson (1987) showed how the olivine tholeiite lavas of Kilauea, Hawaii, behave on this diagram just as would be expected for a magmatic suite fractionating within the upper crust, and therefore controlled by the 1 atm cotectic. Likewise, the ~132 Ma Horingbaai dyke swarms, immediately NW of Spitzkoppe (Thompson *et al.*, 2001) conform closely on this diagram (Fig. 8b) to the expected behaviour of olivine tholeiite magmas fractionating within the upper crust. In contrast, the Spitzkoppe dykes behave very differently (Fig. 8a). Picrites and basalts with >9 wt % MgO form a fan-shaped array, as would be appropriate for compositions controlled by accumulation or removal of olivine. The trend for dykes with lower MgO contents is scattered. Although MgO generally falls

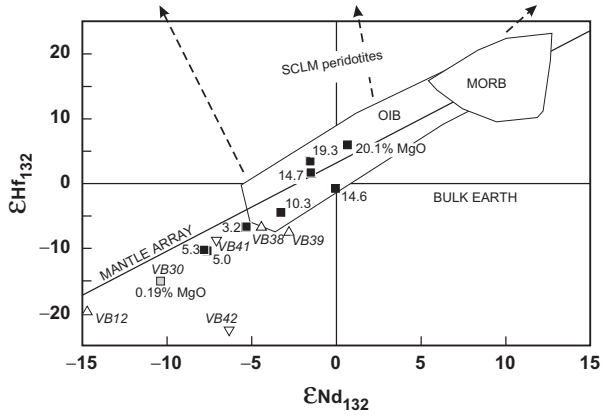

Fig. 6. εNd and εHf in the Spitzkoppe dykes and Damara belt granites and metasediments (at 132 Ma). Symbols and data sources as in Fig. 5. Mantle array and fields for MORB and OIB from Nowell *et al.* (1998), Chauvel & Blichert-Toft (2001), Graham *et al.* (2006) and references therein. Dashed vectors indicate the field of ancient sub-continental lithospheric mantle (SCLM) peridotites (Pearson *et al.*, 2003).

as the Spitzkoppe dyke compositions migrate towards the Qz apex of the diagram, this relationship is not a close one. The non-picritic dyke analyses give the overall impression in Fig. 8a that they lie scattered along a cotectic (or bundle of cotectics) at similar depths to, or perhaps a little deeper than, the one at 0·35 GPa (~14 km depth) marked by the Martindale basalt liquidus phase equilibria (Helz, 1980). This places the likely site or sites for the evolution of the Spitzkoppe dykes within the lower crust. Furthermore, they appear to have evolved at depths less than the ~30–35 km of the Moho in this area (Green, 1983; Miller, 1983; Gladczenco *et al.*, 1997; Bauer *et al.*, 2000) because the compositions do not trend towards alkalic residua, as has been shown experimentally to occur at 0·8–0·9 GPa (Thompson, 1982; Grove *et al.*, 1992). Although some of the natural cotectics for Spitzkoppe dykes seem to be further from the Cpx apex of Fig. 8a than predicted by the closed-system fractional crystallization experimental results of Villiger *et al.* (2007), modelling using pMELTS indicates that this phenomenon appears to be caused by AFC processes involving granitic (*sensu lato*) crust (Fig. 8b and see below). The lavas of the Snake River Plain, Idaho, behave in the same way (Thompson *et al.*, 1983, fig. 1b).

When the radiogenic isotope data are viewed in this light, the trends of the Spitzkoppe dyke analyses in Figs 5–7 can be interpreted with more confidence. Relatively low $^{143}Nd/^{144}Nd$ (negative εNd), $^{87}Sr/^{86}Sr$ and $^{206}Pb/^{204}Pb$ are all characteristic of the high-grade metamorphic rocks that are thought to form the lower half of most continental crust (Moorbath *et al.*, 1975; Dickin, 1981; Scherer *et al.*, 1997; Rudnick & Gao, 2003; Dickin, 2005). The trends for picrite and some of the basalt data in Figs 5 and 7 are therefore clearly compatible with AFC processes at lower-crust depths in the Spitzkoppe dyke suite, as will be discussed further below.

Rhyolite melt evolution in the upper crust?

When their elemental compositions alone are considered, the rhyolite dykes in the Spitzkoppe swarm appear to be part of the same magmatic suite as their picrite–intermediate companions (Figs 3 and 4). The plot of Nd–Hf isotope ratios shows the same relationship (Fig. 6) but the situation becomes subtly different when Sr isotopes are considered. The rhyolite dykes [Table 3 and Frindt *et al.* (2004*b*)] have considerably higher $^{87}Sr/^{86}Sr$ ratios (Fig. 5) than can be fitted by any plausible mixing curve passing through the data for the picritic–basalt dykes. Instead, the rhyolite dykes have $^{87}Sr/^{86}Sr$ ratios in the same range as the metasediments and extensive S-type granites of the Damara belt (McDermott *et al.*, 1989, 1996; McDermott & Hawkesworth, 1990; Jung *et al.*, 2003), the regional rock-types into which they are emplaced. Lead isotopes (Fig. 7) show a subtly different relationship. Both the rhyolitic and two of the accompanying Mg-poor basaltic dykes lie within the compositional fields of the Damara S-type granites and metasediments. Figures 5 and 7 also show how relatively high $^{87}Sr/^{86}Sr$ and $^{208}Pb/^{204}Pb$ separate the Spitzkoppe rhyolite dyke compositions from those of the granites in the penecontemporaneous Gross Spitzkoppe stock, around which they are emplaced. The simplest way to interpret these isotopic relationships is to deduce that the picritic–magnesian basalt magmas of the Spitzkoppe swarm evolved within the lower or middle crust and the rhyolite melts developed by extreme AFC at upper-crust levels. Nevertheless, localized wholesale upper-crustal melting cannot be ruled out. The Mg-poor and intermediate dyke magmas followed a complicated series of individual paths through the sub-Spitzkoppe continental crust.

Modelling the fractional crystallization

Open-system fractional crystallization in the Spitzkoppe magma system can be confirmed by means of modelling calculations using MELTS, pMELTS and Adiabat_1ph (Smith & Asimow, 2005), as detailed in the Appendix. Apart from traces of interstitial biotite (Table 1) in the thickest picrite dykes—with the volatiles probably inherited from traces of hydrous minerals in the SCLM (see below)—the mineralogy of all the Spitzkoppe dykes is anhydrous. The only exception is a trace of interstitial blue–green amphibole in rhyolite VB30. It therefore seems a reasonable approximation to treat the Spitzkoppe magma system as anhydrous until further research clarifies its water content.

Method. All the picrite dykes are olivine-phyric and limited microprobe study suggests that the olivine is accumulative (Fig. 2). Attempts to model fractional crystallization using the original version of MELTS, however,

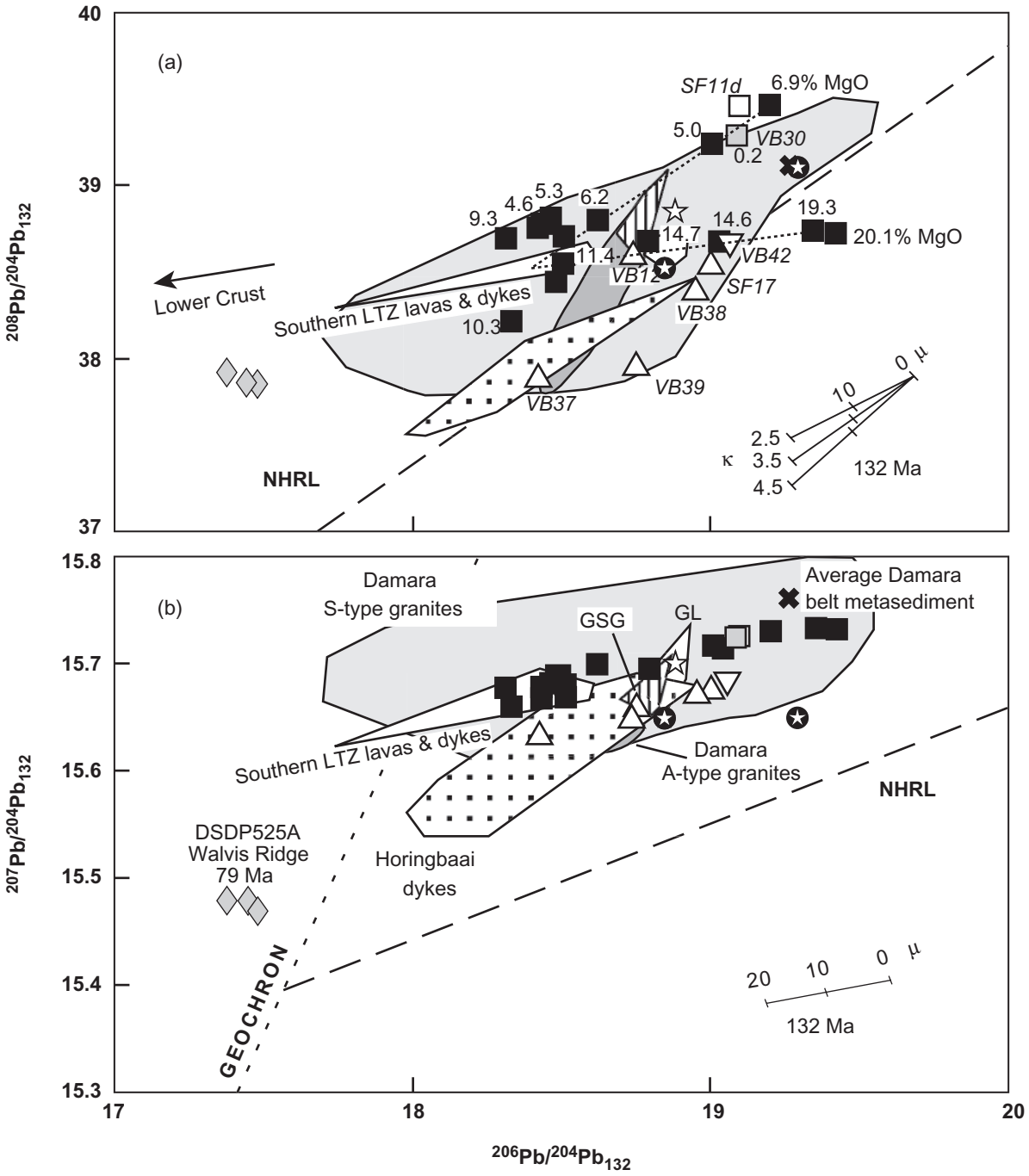

Fig. 7. Initial $^{206}Pb/^{204}Pb$, $^{207}Pb/^{204}Pb$ and $^{208}Pb/^{204}Pb$ in Spitzkoppe dykes and Damara belt granites and metasediments (at 132 Ma). Symbols and data sources as in Fig. 5. The dotted lines show trends in Pb isotopic ratios in the dykes. Polygonal fields are from Thompson *et al.* (2001), Ewart *et al.* (2004*a*) and Frindt *et al.* (2004*b*). Average Damara belt metasediments from McDermott & Hawkesworth (1990). GSG, Gross Spitzkoppe granite; GL, Goboboseb quartz latites. Northern Hemisphere Reference Line (NHRL) from Hart (1984). Vectors illustrate the 132 Ma correction for different values of μ and κ.

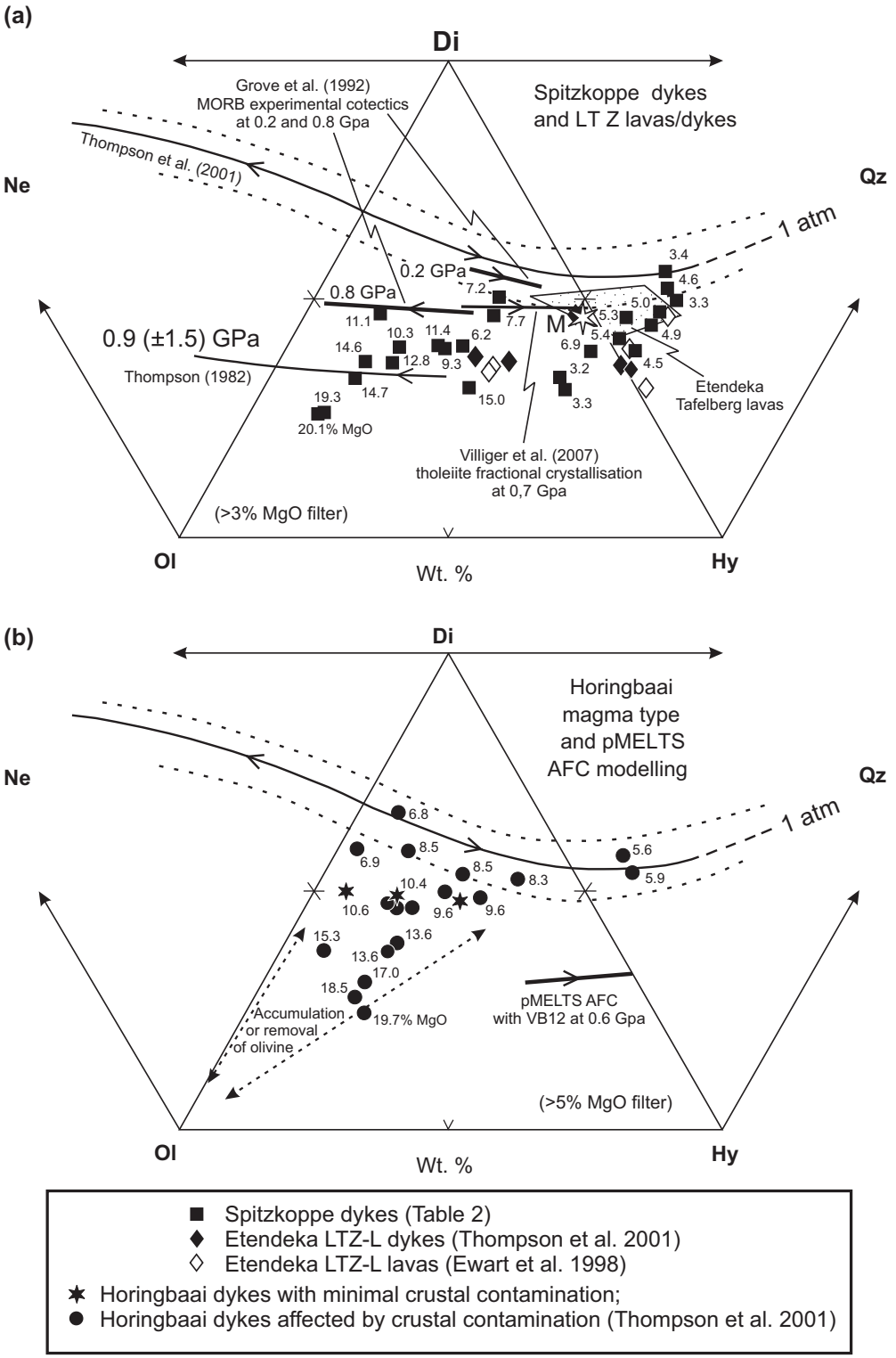

Fig. 8. CIPW normative diopside, olivine, hypersthene, nepheline and quartz in Spitzkoppe dyke samples and comparisons. All data are calculated with 10% of total iron as Fe_2O_3. (Thompson & Gibson, 2000). Cotectics at 1 atm, 0·2, 0·7, 0·8 and 0·9 GPa for the equilibrium [ol + plag + cpx + basaltic liquid] are from Thompson (1982), Grove *et al.* (1992), Villiger *et al.* (2007) and the data of Sack *et al.* (1987); arrows mark directions of falling temperature. The continuous-line 1 atm cotectic is the best fit to the experimental data; all of the latter fall between the dashed lines. The pMELTS cotectic for AFC involving Damara granite VBl2 (see text) is from pMELTS modelling in this paper. (a) Spitzkoppe dykes (MgO >3·0 wt %) and southern Etendeka Tafelberg lavas and LTZ-L lavas and dykes (Erlank *et al.*, 1984; Ewart *et al.*, 1998*a*; Thompson *et al.*, 2001). MgO contents are marked beside dyke points. (b) Horingbaai dykes (Thompson *et al.*, 2001). MgO contents are marked beside most points.

predicted extensive liquidus orthopyroxene. It is known (Table 1) that at least picrites VB18 and 32 contain small amounts of interstitial orthopyroxene; their bulk compositions are thus not far from saturation with this phase. The original MELTS algorithm overestimated the relative stability of orthopyroxene compared with olivine (Hirschmann *et al.*, 1998) and it is perhaps unsurprising that this systematic bias is enough to stabilize the 'wrong' phase. Although it is intended for calculations at >1 GPa, and for peridotite compositions only, pMELTS sometimes captures the behaviour of MgO-rich basaltic melts (*sensu lato*) more closely than MELTS (e.g. Smith *et al.*, 2003). Hence, we repeated the calculations using pMELTS, which gave olivine as the liquidus phase. We stress that because (with the exception of the 1 GPa result) the calculated trends lie outside the calibrated range of the pMELTS model, the quantitative results should be taken with some caution.

The most MgO-rich aphyric dyke sample in this suite is VB26 (11·09 wt % MgO) although, as discussed in the 'Focus on the picrites' section below, the real parental melts at Spitzkoppe may have had as much as 15–20 wt % MgO. The usual way in which algorithms such as (p)MELTS are employed to model fractional crystallization is to select a putative parental composition from the samples in the magmatic suite, such as VB26, and then to use the software to predict how this might undergo fractional crystallization, or AFC if required, under various P–T regimes. This approach means that elemental abundances in the calculated evolving melt are forced to be the observed values and any mismatch between parameterized and actual phase compositions must be taken up by the solid phases only, which sometimes causes the predicted melt to evolve to extreme compositions. In contrast, when (p)MELTS is used for melting calculations, the bulk composition is imposed and any mismatches between actual and predicted phase compositions are distributed over all the phases present. Consequently, rather than using the natural dyke chemical analysis of VB26 as the starting composition for fractional crystallization modelling, it was preferable to use pMELTS to generate a picrite 'model parental melt', which (according to pMELTS) could then fractionate olivine alone until it closely resembled VB26.

Extensive trial-and-error mantle fusion calculations with pMELTS produced a suitable 'model primary melt'. This aggregated fractional melt, with ~20 wt % MgO, was generated by isentropic decompression melting under a relatively thin lithospheric lid. For Os-isotope reasons explained below, depleted mantle compositions such as those from McKenzie & O'Nions (1991, 1995) and Workman & Hart (2005) were tried and the best fit was achieved by using the former with the potential temperature (T_p) of the mantle set to ~1500°C. The 'model parental melt' was derived by subtracting olivine fractionally from the 'model primary melt' until MgO reached ~15 wt % (the lower limit of the estimated primary magma range, with a calculated equilibrium olivine of Fo_{90}). The actual trace-element abundances and isotopic ratios of VB19 were attached to 'model VB19' (Table 2). Of the three picrite dykes with similar MgO contents, VB19 was chosen for its wide range of isotope determinations and because its trace-element abundances were close to the average values of the other two (i.e. VB3 and 18).

It is conceivable that parental magmas were transported laterally as dykes from a location near the axis of the Proto-Atlantic rift, where the lithosphere would have been thinner (e.g. Bauer *et al.*, 2000), but obviously the pMELTS starting model cannot be used to discuss in detail the ultimate origin of the Spitzkoppe picrites. It is simply a device to let the pMELTS algorithm interact with a 'starting composition' that it 'recognizes' as having been originally in equilibrium with a lherzolite mantle.

AFC

Bowen (1928) concluded that, because upwelling magma is generally porphyritic, most magmas are saturated and carry little or no superheat. Therefore heat for dissolving country rock comes from that released during crystallization of the melt. As his detailed phase-diagram approach demonstrated, however, the reaction progression depends on the complicated interactions of temperature-dependent phase stability fields. Hence, AFC is ideally suited for analysis with a thermodynamically based model, such as MELTS, and we have applied the Adiabat_1ph front-end here also.

For the Spitzkoppe suite it has been necessary to modify the procedure in several ways and new features were added to the public version of Adiabat_1ph in the process; details are given at www.gps.caltech.edu/~asimow/adiabat and in the Appendix. This included an implementation of isenthalpic calculations together with a means to specify the thermal state of the assimilant. The initial crustal temperature was taken as 500°C after considering Cretaceous palaeogeothermal gradients derived from lherzolite mantle xenolith P–T equilibria from Okenyenya (Baumgartner *et al.*, 2000) and near Swakopmund (Whitehead *et al.*, 2002), the two nearest appropriate localities. The starting situation was 100 g of 'model VB19' at its liquidus, and fifty 1 g increments of either VB12 or PA19 acid crust (see Fig. 9 legend) were added.

Reiners *et al.* (1995) incorporated the original software of Ghiorso & Sack (1995) into a quantitative model of heat-balanced AFC and showed that the ratio of the rates of assimilation and fractional crystallization, r, could vary dramatically as a typical magma evolved. Naturally, cooling and magma transport rates can strongly affect the r value (e.g. Kuritani *et al.*, 2005) and very complex models of magma chamber processes, such as the

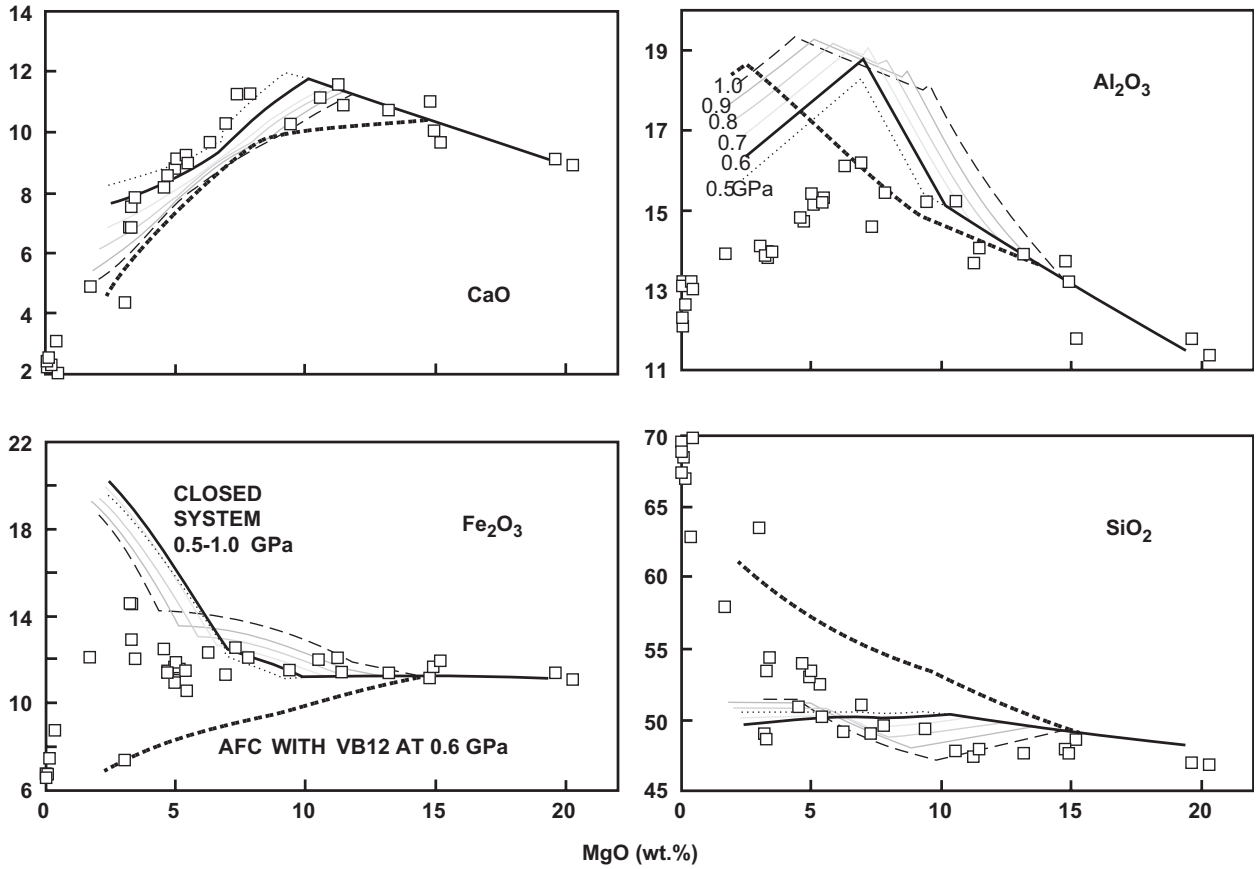

Fig. 9. Variations of CaO, Al_2O_3, Fe_2O_3 and SiO_2 in the Spitzkoppe dykes as functions of MgO. Also plotted are closed-system fractional crystallization and AFC trends modelled using pMELTS. Details of the modelling are given in the text; each trend-line is based on ~310 modelling steps for fractional crystallization and ~50 steps for AFC. Closed-system modelled fractionation curves at various anhydrous pressures are labelled in the Al_2O_3 plot. The 0·6 GPa curve (bold continuous line) gives the best fit to the dyke CaO and Al_2O_3 analyses. The AFC modelled trend using Damara granite VB12 (Fig. 1) is shown as a bold dashed line; the trend using Paresis rhyolite PA19 approximately overlies this one.

EC-E'RAχFC model of Spera & Bohrson (2004), can be developed if all likely factors are included. Here a relatively simple equilibrium model was used and the calculations were undertaken in two stages, which represented extreme cases. First, the magmatism was treated as closed-system fractional crystallization of a cooling dry parental magma. Second, the thermal evolution during AFC was constrained by balancing the heat released during fractional crystallization with that required to melt and incorporate plausible country rock. This latter case is approximately equivalent to the 'maximal contamination' end-member of Spera & Bohrson (2004) and assumes no heat loss by conduction.

Results. Using the procedure described above, pMELTS calculated the closed-system fractional crystallization trends shown in Fig. 9. Examples at pressures between 0·5 and 1·0 GPa are plotted and compared with the Spitzkoppe dyke data. The variation in the calculated MgO–CaO inflexion with pressure is relatively small and thus the inferred pressure is only loosely constrained, especially given our caveat about extrapolating pMELTS. It is encouraging, however, that the bold continuous line corresponding to a pressure of 0·6 GPa, which is in the middle of the range inferred qualitatively from Fig. 8 (~0·35–0·8 GPa), falls closest to most of the Spitzkoppe data for CaO and Al_2O_3. At higher anhydrous pressures, spinel precipitated in the pMELTS models (see Fig. 9) and this phase is not observed in any Spitzkoppe dykes.

For comparison, the model results for adding granitic crust VB12 during AFC of 'model VB19' at 0·6 GPa are shown (dashed line) in Fig. 9. Results for adding Paresis rhyolite PA19 (Mingram *et al.*, 2000), the proxy for lower-crust partial melt used in this paper, are almost identical. For most oxides the data fall between the closed-system and open-system curves, suggesting that AFC processes dominated the dyke evolution but that the *r* value was lowered by conductive heat loss. This is particularly clear in the FeO* plot, which shows that Fe–Ti oxides reached saturation below ~7 wt % MgO in the dyke magma and AFC models but not in the closed-system models,

in agreement with the experiments of Villiger *et al.* (2007). With the exception of Al_2O_3, the fit to all oxides (including P_2O_5 and TiO_2, which are not shown) is good and reinforces our confidence in the ability of pMELTS to describe Mg-rich basalt evolution. We tested the possibility that small amounts of water in the parental melts—such as might be held in the minerals of nominally anhydrous mantle (Hauri *et al.*, 2006)—was the reason for the poor Al_2O_3 fit by re-running the 0·6 GPa calculations using pHMELTS and H_2O contents up to 1 wt %. The misfit for Al_2O_3 became worse and therefore remains unexplained. This is clearly a limitation to the complete success of the modelling.

The success of pMELTS in modelling the isotopic consequences of AFC is clear in Fig. 5. The model curves are marked with increments of added crust in grams (see the Appendix). This is close to, but not identical to, added crust marked as percentages. Starting from 'model VB19', the AFC curve in Fig. 5 involving Paresis rhyolite PA19 (Mingram *et al.*, 2000) is consistent with the concept that fractionation from parental to less Mg-rich Spitzkoppe picrites also involved AFC interaction with melts from ancient granulite-facies lower crust below Spitzkoppe. The AFC curve involving local Damara belt granite VB12 (Table 2) passes through the Sr–Nd isotopic ratios of Spitzkoppe basaltic and intermediate dykes. Its curvature is very similar to that of the simple mixing curve in Fig. 5 described previously but this is made harder to see by the two curves having different origins—VB32 for the mixing curve and 'model VB19' for the AFC curves. The advantage of using the pMELTS algorithm over the simple mixing calculation is that a single model can simultaneously describe the variations in major and trace element abundances (see Fig. 16 and discussion below) as well as isotopic variations.

Magma densities and crustal magmatic plumbing

Figure 10 summarizes how various radiogenic isotopic ratios in the Spitzkoppe dykes behave as functions of MgO. The published isotopic ranges for Damara belt pre-Cretaceous crustal rock-types exposed at the surface are also given for comparison (double-headed grey arrows), together with our new data (Table 3). Where significant sections of the dyke data show good linear trends, these have been fitted by least-squares regressions. This diagram emphasizes how the $^{206}Pb/^{204}Pb$ data for dyke compositions between 20 and 9 wt % MgO follow trends away from the composition range of the exposed Damara belt crust. The $^{207}Pb/^{204}Pb$ and $^{208}Pb/^{204}Pb$ trends are the same but with a lower R^2. Although $^{207}Pb/^{204}Pb$ and $^{208}Pb/^{204}Pb$ are relatively low in Damara crust samples VB37 (pegmatite alkali feldspar) and VB39 (aplite), it is clear from Fig. 10 that their extremely high $^{87}Sr/^{86}Sr$ ratios rule these rock-types out as responsible for the Pb isotope trends. Between 9 and 3 wt % MgO the majority of the dykes have similar, or slightly higher, $^{206}Pb/^{204}Pb$, $^{207}Pb/^{204}Pb$ and $^{208}Pb/^{204}Pb$ ratios to the basalts with ~10 wt % MgO. A minority of this dyke group is isotopically distinctive, with $^{206}Pb/^{204}Pb > 19·0$, $^{207}Pb/^{204}Pb > 15·71$ and $^{208}Pb/^{204}Pb > 39·2$, as in rhyolite VB30. In contrast, the $^{143}Nd/^{144}Nd$ and $^{176}Hf/^{177}Hf$ linear trends extend throughout the dyke compositions, from picrite to rhyolite. Finally, the complicated behaviour of $^{87}Sr/^{86}Sr$ helps to explain the other isotopic data. Between 20 and 10 wt % MgO, the picrites and olivine-basalts show no significant variation in $^{87}Sr/^{86}Sr$ with falling MgO. Below 10 wt % MgO, $^{87}Sr/^{86}Sr$ in the dykes rises irregularly to values similar to those in Damara belt upper-crustal rock-types.

If, as we argued above, the fall in MgO between picrites and rhyolites in the Spitzkoppe dykes is due to AFC fractional crystallization, then the progressive changes in isotopic ratios through the suite must logically be linked to the same process, AFC, with the contaminant varying progressively as MgO falls. At first sight this sounds impossible because the microprobe studies (Fig. 2) show that the picrites are cumulates. How could the process of crystal accumulation have anything to do with changing radiogenic isotopic ratios? A possible link can be found in the densities of the magmas. In Fig. 11 all the dyke compositions, including the picrites, have been treated as liquids of equivalent compositions. This simplification avoids considering the picrites as liquid–solid suspensions. It is difficult to do otherwise because of the problems associated with estimating what proportion of the margins of their olivine phenocrysts crystallized during their uprise and emplacement. The effect of this simplification is to underestimate the pre-emplacement densities of the picrites, relative to the phenocryst-poor more evolved magmas. No crystal sorting during and after dyke emplacement is also assumed, and this is another considerable simplification.

The melt densities for each dyke in Fig. 11 were calculated from their partial molar volumes, taking no account of pressure and reducing melt temperature in steps from 1250°C in the picrites to 1000°C in the rhyolites. The resulting melt densities fall progressively from picrites to rhyolites. Therefore, in a sense, Fig. 11 may be seen to show systematic changes in the radiogenic isotopic ratios of the Spitzkoppe dykes with the densities of the magmas. This might occur if each dyke tapped from various depths a fractionating magmatic system in which the density of the melts varied vertically. Such a magmatic system would be stable in a crust with similar vertical density variations to the magmas, so that the relative buoyancy of all the melts was similar. Figure 11 shows that this situation could be achieved if, for instance, the sub-Spitzkoppe crust resembles that of the well-studied northern

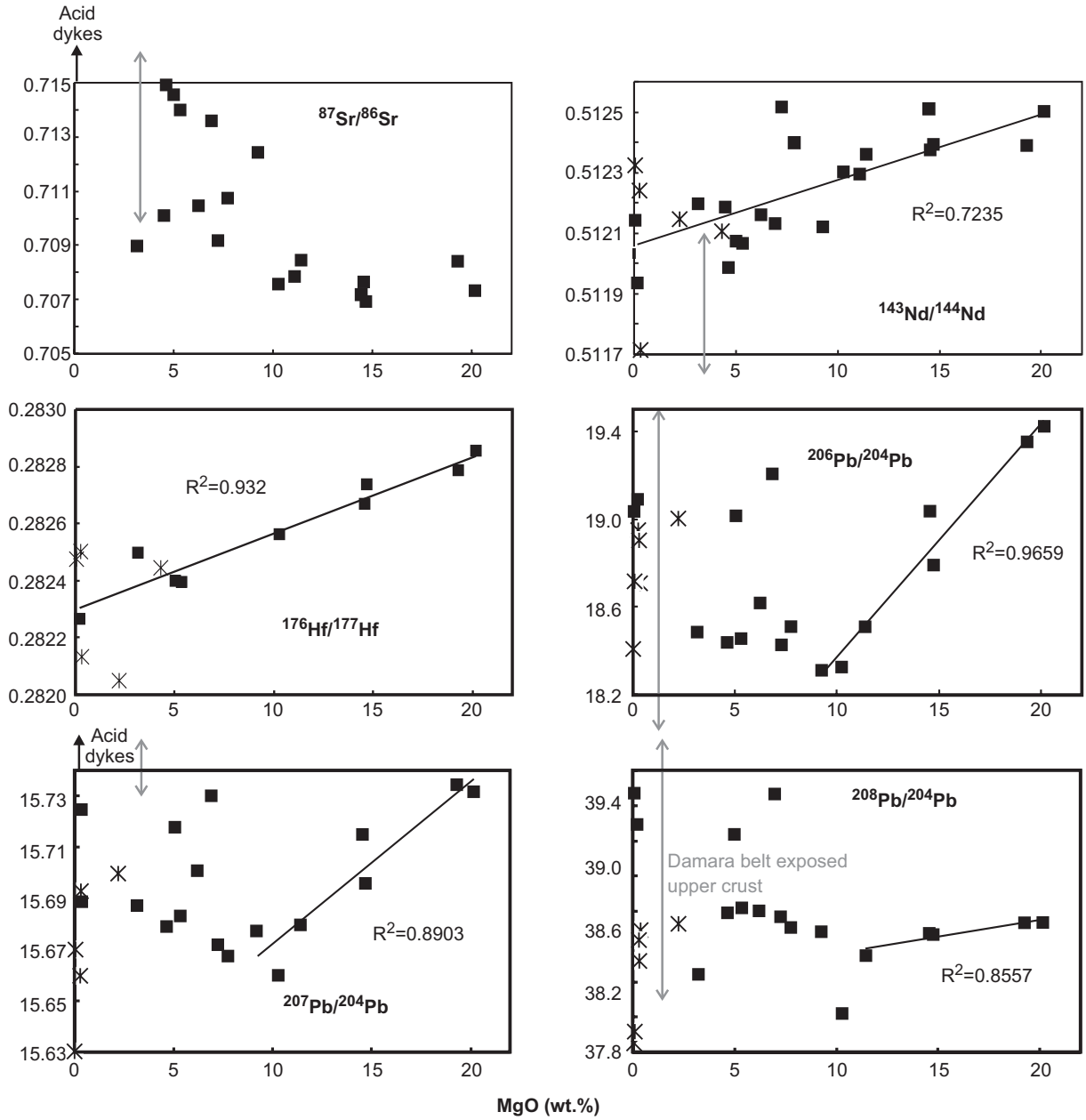

Fig. 10. Variations of Sr, Nd, Hf and Pb isotopes in the Spitzkoppe dykes ({squf}) as functions of MgO. In the Pb isotope plots, Durham data are used for the dykes and McMaster data for the Damara crustal rocks (Table 3). Trend lines are least-squares regressions through dyke analyses; only analyses with >9 wt % MgO for Pb isotopes. Crosses are new analyses of Damara belt rock-types (Table 3). Double-headed grey arrows are published Sr, Nd and Pb isotopic ratio ranges for Damara belt exposed upper crust (McDermott *et al.*, 1989, 1996; McDermott & Hawkesworth, 1990; Jung *et al.*, 2003). There are no published Hf isotope ratio data for these rock-types. The new analyses (Table 3) extend the published ranges for several isotopic ratios.

Scotland region, where Proterozoic metasediments overlie an Archaean middle and lower crust, within which the metamorphic grade varies downwards from amphibolite facies to granulite facies.

There is no seismic study of the crust immediately below Spitzkoppe but this region falls between the two detailed seismic transects of Bauer *et al.* (2000), about 70 km NW of the eastern end of Transect 2. All the onshore part of this transect shows a laterally uniform crustal seismic structure, with P velocities increasing progressively from 6·1 km/s at ~6 km to 6·7 km/s at ~33 km depth. The calculated equivalent rock densities (Christensen & Mooney, 1995) are shown in Fig. 11. These form a similar array to the MOIST data (Fig. 11) but at slightly higher densities.

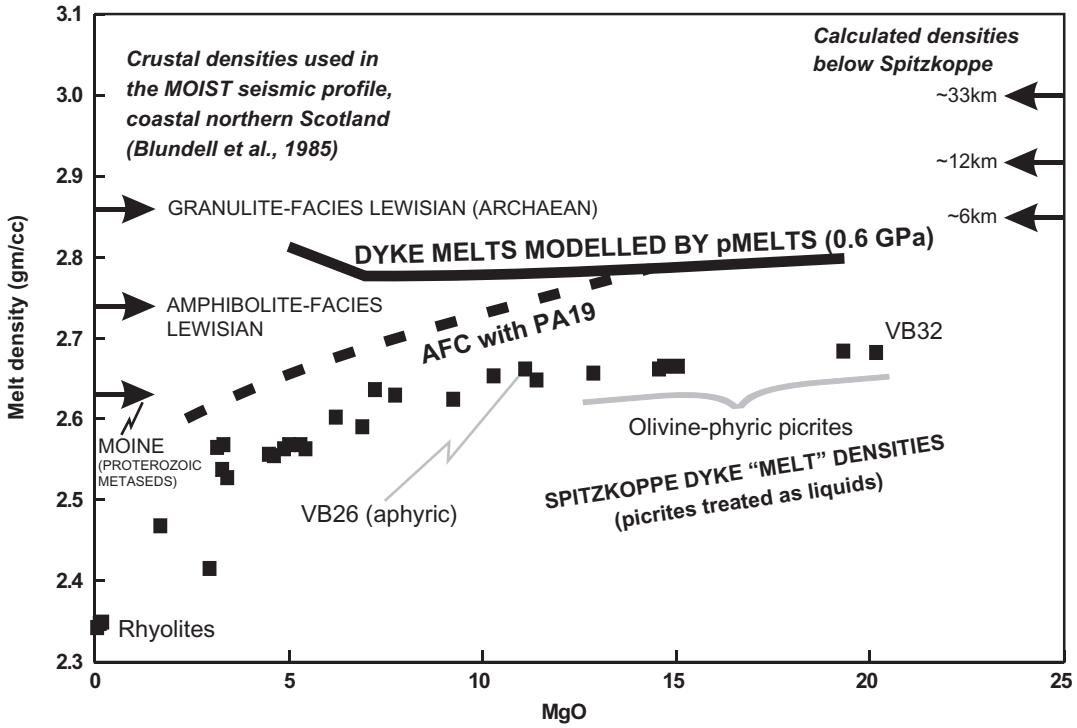

Fig. 11. Calculated densities of Spitzkoppe dyke melts and of analogue melts modelled using pMELTS. The modelling is for closed-system anhydrous fractional crystallization (continuous line) and for AFC using Paresis rhyolite PA19 (dashed line) as the contaminant—both at 0·6 GPa. (See text for details of modelling and reasons for using PA19.) All Spitzkoppe dyke compositions treated as liquids, including porphyritic samples (see text). Comparative densities for Archaean granulite- and amphibolite-facies acid–intermediate gneisses, and for Proterozoic metasediments, are taken from the MOIST seismic profile along the northern coast of Scotland (Blundell *et al.*, 1985). Crustal densities below Spitzkoppe are calculated (Christensen & Mooney, 1995) from the crustal P seismic velocities at the eastern end of Transect 2 of Bauer *et al.* (2000), ~70 km SE. The estimated sub-Spitzkoppe Moho depth is ~35 km.

Nevertheless, the base-of-crust P velocity is below the values corresponding to mafic igneous rocks. In contrast, about 100 km offshore from NW Namibia the upper crust becomes strongly attenuated and, below ~11 km depth, P velocity rises from 7·2 to >7·6 km/s and contains seaward-dipping seismic reflectors (Bauer *et al.*, 2000). Cretaceous palaeotemperatures calculated from mineral equilibria in peridotite xenoliths from localities ~100 km NE and SW of Spitzkoppe, respectively, are ~1000°C for xenoliths derived from the mantle immediately underlying the Moho (Baumgartner *et al.*, 2000; Whitehead *et al.*, 2002). Therefore is very likely that the lower crustal Cretaceous palaeotemperatures below Spitzkoppe were high enough to maintain granulite-facies metamorphism.

Melt densities were also calculated during the magma modelling using pMELTS, described above. The closed-system fractionation and open-system (AFC) results for 0·6 GPa are plotted as continuous and dashed trend-lines in Fig. 11. The model AFC trend clearly fits the dyke data well. If the dyke magmas came from a fractionating system in which the picrites resided in the lower crust and the rhyolites in the upper crust, then the Sr isotope data in Fig. 10 can be understood. Ancient acid–intermediate granulite-facies metamorphic rocks—characteristic of the lower crust in many continental regions (e.g. Rudnick & Gao, 2003)—typically have relatively high Sm/Nd, and low Lu/Hf, Rb/Sr, U/Pb and Th/Pb (Moorbath *et al.*, 1975; Dickin, 1981, 2005; Scherer *et al.*, 1997), thus accounting for the distinctive AFC trends of the Spitzkoppe dyke magmas with >10 wt % MgO. Likewise, the acid magmas match isotopically the Damara belt exposed Proterozoic–Cambrian metamorphic rocks and granites. Between these extremes some of the Spitzkoppe dykes with 3–9 wt % MgO seem to have been reacting with crust that had similar Nd–Hf–Pb isotopic characteristics to the lower crust, but with relatively higher time-integrated Rb/Sr. Amphibolite-facies middle crust would fit this isotopic profile well (Dickin, 1981).

Clearly, it is possible to construct other speculative scenarios where, for instance, the metamorphic grade of

the crust varies laterally. The chosen situation is the one that best fits published seismic data. Finally, it is important to stress that neither Fig. 10 nor the other isotopic plots specify the physical paths taken by individual dyke magmas. Thus a dyke with, say, 7 wt % MgO could: (1) be melt that completed AFC evolution in the middle crust, having previously followed a different AFC path as it rose through the lower crust; (2) have a parent melt that rose directly from the mantle to stagnate within the middle crust.

Figure 12 is a schematic illustration intended to summarize and clarify the concepts developed above, together with ideas discussed in the section below, which focuses on the sources of the Spitzkoppe picrites. The structure of the sub-Spitzkoppe crust is extrapolated from extensive seismic and gravity sections passing north and south of the area (Bauer *et al.*, 2000). These are concordant with previous seismic studies (Green, 1983; Miller, 1983; Gladczenko *et al.*, 1997). An unusual feature of this seismic structure is the lack of any significant amounts of mafic lower crust (V_p >7·0 km/s), as emphasized above. This means that it is reasonable to suppose that intermediate and possibly some acid granulite-facies metamorphic rocks (of either igneous or sedimentary parentage) dominate the lower crust below Spitzkoppe.

The mafic dykes may originally have been emplaced laterally—possibly from the zone of thinned lithosphere marking the eventual South Atlantic rift (Gladczenko *et al.*, 1997; Bauer *et al.*, 2000; Thompson & Gibson, 2000). Nevertheless, the combined volume of the Gross and Klein Spitzkoppe granite stocks suggests strongly that a substantial local magmatic system developed below Spitzkoppe. This system could either have fractionated by AFC directly to the magmas that produced the granite stocks or provided the heat that generated them by upper-crust melting. The oxygen isotope evidence of Harris (1995) and Trumbull *et al.* (2004*a*) favours the latter model for the granites but the differences in Sr, Nd and Pb isotopic ratios between the rhyolite dykes and the Gross Spitzkoppe granite favours the view that even the acid dykes around Spitzkoppe have a different origin from the granites, as extreme AFC products.

Elsewhere beneath the Etendeka igneous province, such local systems may have developed very large intra-crustal magma chambers—sufficient to fuel the eruption of the enormous quartz latites (e.g. Milner *et al.*, 1995; Ewart *et al.*, 2004*b*). Around Spitzkoppe the remarkably complete picrite–rhyolite suite of dykes, each with their distinctive geochemistry, argues against the homogenizing effects of a large magma reservoir. The preferred model is a stack of sills and their interconnecting dykes and/or pipes, allowing an overall magmatic evolution column to be tapped from a range of depths throughout the crust, as proposed for magmatism elsewhere (Thompson *et al.*, 1972; Morrison *et al.*, 1985; Marsh, 2004; Thompson *et al.*, 2005). It should be noted that the Spitzkoppe picrites form by far the thickest dykes. Presumably exceptionally intense extension events were required to tap such dense and deep magmas. Finally, the summaries of isotopic characteristics at each level in Fig. 12 are, of course, not directly observed but deduced from reasoning outlined above.

FOCUS ON THE PICRITES

In all the diagrams above where geochemical data are plotted the picrites, notably sample VB32, form the mafic end-members to the Spitzkoppe dyke suite. Nevertheless, it is clear from Fig. 2 that the high MgO content of the picrites is not an indication that they were emplaced as exceptionally Mg-rich liquids. Instead, their high MgO contents reflect accumulation of olivine phenocrysts in liquids that, judging from the compositions of the aphyric members of the suite and the calculated equilibrium liquids, did not exceed ~11 wt % MgO. This contrasts with the picrites in the penecontemporaneous dyke swarms around Brandberg and the Huab area to the NW (Fig. 1, inset), which frequently contain olivine phenocrysts more forsteritic than Fo_{91} (Fig. 2), rising exceptionally to $Fo_{93·3}$ (Thompson & Gibson, 2000; Thompson *et al.*, 2001). The sampling of Spitzkoppe picrites to date (Table 1) is insufficient to be certain that equally forsteritic olivine phenocrysts do not occur. Alternatively, the magmatic plumbing of the Spitzkoppe system may have prevented extremely Fo-rich olivine reaching the upper crust. It therefore seems prudent to suspect that the parental melts fuelling the Spitzkoppe system probably included liquid compositions with MgO in the 15–20 wt % MgO range, but that these were not emplaced unmodified.

The radiogenic isotopic ratios (crucially excluding Os; see below) of the four picrites studied in detail, VB11, 18, 19 and 32, are appropriate to a convecting mantle source similar to those of OIB (Figs 5–7), with $^{87}Sr/^{86}Sr$ ~0·707, εNd ~0, εHf ~+2·5, $^{206}Pb/^{204}Pb$ ~19·16, $^{207}Pb/^{204}Pb$ ~15·70 and $^{208}Pb/^{204}Pb$ ~38·67 (Table 3). In contrast, the elemental compositions of the samples are very different from either MORB or OIB. These differences are illustrated by a normalized plot of the abundances of a range of elements in the picrites (Fig. 13). In Fig. 13a the contrast between the 'spiky' Spitzkoppe patterns and average enriched MORB (E-MORB; Sun & McDonough 1989) is clear. It is also interesting to see how similar the E-MORB pattern is to that of a Horingbaai basalt dyke (97SB29) that appears to have undergone minimal crustal contamination (Thompson *et al.*, 2001). Figure 13b shows that duplicate chemical analyses of samples VB11 and 32, from the same Black Range picrite dyke, vary negligibly. In the right-hand part of the diagram, between Sr and Lu, the inter-element ratios of the picrites are similar to those of normal MORB (N-MORB; Sun & McDonough, 1989),

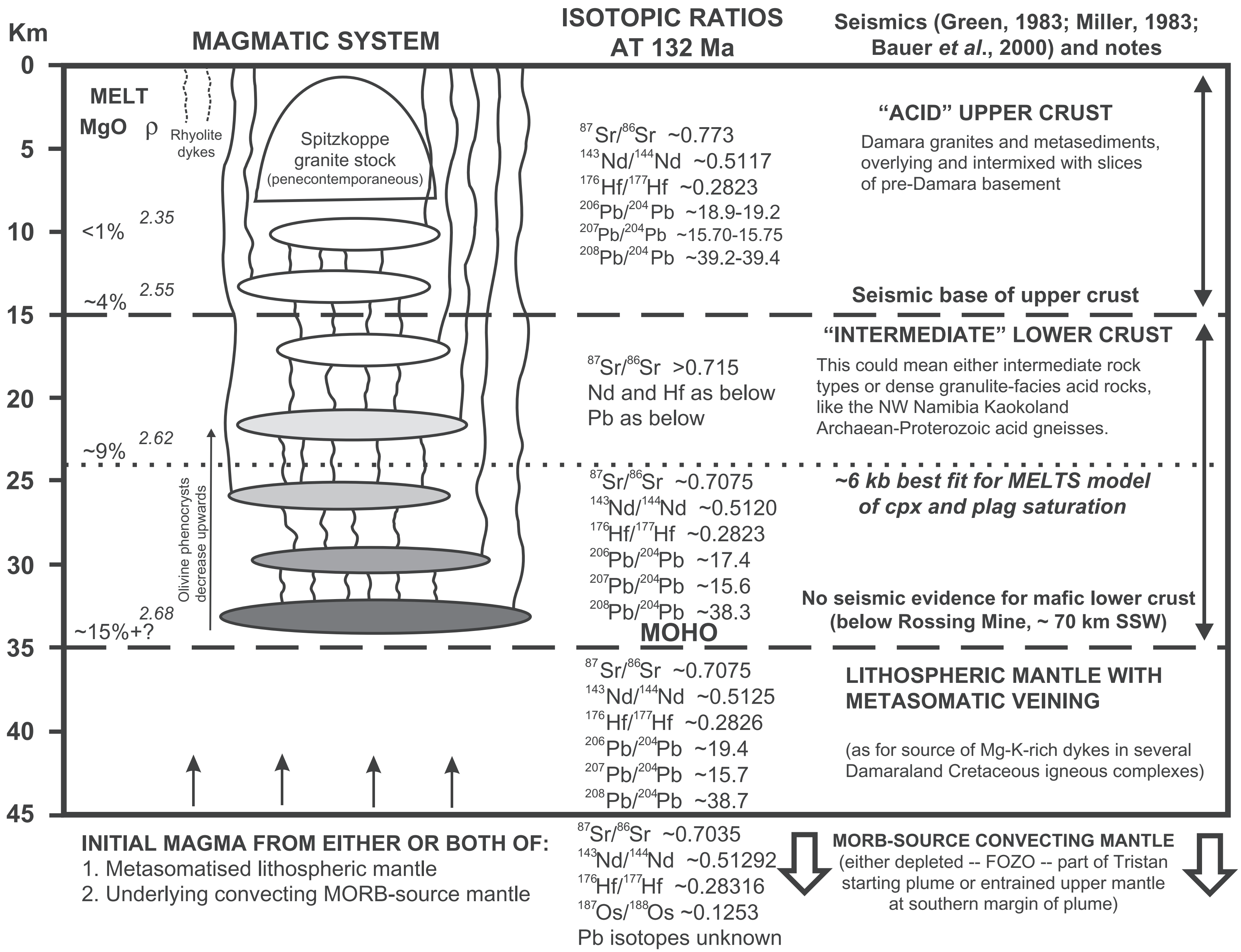

Fig. 12. Schematic illustration interpreting all the available data on the Spitzkoppe dyke suite geochemistry and the geophysical structure of the underlying crust. The schematic sill–dyke complex is the simplest scenario to accommodate all the factors discussed in the text. Shading indicates the relative abundance of olivine phenocrysts in the cumulate picrite lower-crust sills. The sills indicated within the SCLM are a possible means of introducing some SCLM geochemical characteristics into the parental picrites (see text). The isotopic data summarized in Fig. 10 imply that the actual magmatic plumbing beneath the Spitzkoppe area was much more complex than this illustration shows.

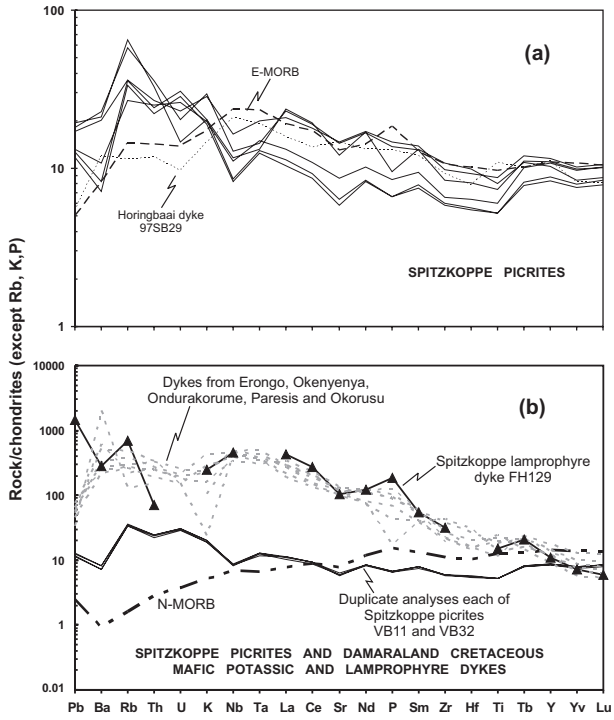

Fig. 13. (a) Normalized (Thompson *et al.*, 1984) elements in Spitzkoppe picrite dykes. Patterns for MORB (Sun & McDonough, 1989) and a Horingbaai picrite dyke (Thompson *et al.*, 2001*l*) are shown for comparison. (b) Patterns for Mg-rich potassic and similar lamprophyric dykes within early Cretaceous Damara belt intrusive complexes (le Roex & Lanyon, 1998; Thompson *et al.*, 2001*l*; Gibson *et al.*, 2005). Four analyses of the Black Rock dyke (Fig. 1, VB11 and VB32) illustrate analytical precision.

whereas all elements in the left-hand part of Fig. 13b show relative enrichment above MORB values.

Osmium isotopes in the olivine phenocrysts of the Spitzkoppe picrites provide another way of discovering a feature of their original compositions. This is because the Os contents of olivine phenocrysts in the Spitzkoppe and Horingbaai dykes range from ~800 to 8000 ppt Os (D. G. Pearson and R. N. Thompson, unpublished data). These values are ~15–150 times higher than average crustal values (Saal *et al.*, 1998) and sufficient to make them very resistant to significant change by the addition of a small amounts of crust. Therefore the Os isotopes of the Spitzkoppe picrites should 'see through' any subsequent crustal contamination that may have affected them and retain values reflecting their equilibria with mantle rocks. Using an emplacement age of 132 Ma, the initial $^{187}Os/^{188}Os$ ratios of the picrite olivines (Table 4) are 0·126248 (VB32) and 0·124262 (VB18). Convincing $^{187}Os/^{188}Os$ ratios for MORB are notoriously hard to obtain and values for abyssal peridotites are usually quoted instead. Nevertheless, Gannoun *et al.* (2004) used mineral isochrons to obtain initial $^{187}Os/^{188}Os$ ratios of 0·1265 and 0·1290 for two Atlantic MORBs, at the lower end of the published range for MORB glasses (Alard *et al.*, 2005). The $^{187}Os/^{188}Os$ ratios of the Spitzkoppe picrites and their olivine phenocrysts, and the Atlantic MORBs, are all well below the range for Atlantic OIB (Hauri, 2002). They are also slightly above the total range (at 132 Ma) for southern Namibian SCLM xenoliths and well above the average value of 0·11781 at 132 Ma (Pearson *et al.*, 2004).

It has been clear throughout the foregoing discussion that the Black Range picrite (samples VB11 and 32; 19–20 wt % MgO) is isotopically the Spitzkoppe magma furthest removed from all observed and inferred crustal compositions in that region. How can this be if its elemental composition differs from MORB in ways that can be modelled satisfactorily by addition of a few per cent of crust to a MORB picrite melt (Fig. 13)? There is an alternative long-standing and popular view that the differences between these Etendeka-related picrites and MORB-source magmas were caused by the picrite sources being located entirely within veined and metasomatized SCLM (e.g. Marsh *et al.*, 1997, 2001*l*; Trumbull *et al.*, 2004*a*). There is limited direct evidence of the nature of the SCLM beneath the Damara belt, in the form of suites of SCLM xenoliths sampled by Cretaceous magmatism at Okenyenya and near Swakopmund (Baumgartner *et al.*, 2000; Whitehead *et al.*, 2002). The closer Swakopmund xenoliths lack evidence of modal metasomatism and pyroxenite veining (Whitehead *et al.*, 2002).

On the other hand, indirect evidence for veined and/or metasomatized SCLM beneath the Damara belt is widespread. Alkaline lamprophyric mafic and ultramafic dykes occur in the majority of the Damara belt Cretaceous intrusive complexes: Okenyenya, Erongo, Ondurakorume and Okorusu (Milner & le Roex, 1996; le Roex & Lanyon, 1998; Thompson *et al.*, 2001*l*); Paresis (Gibson *et al.*, 2005); cutting the Spitzkoppe granite (Frindt *et al.*, 2004*a*); between Spitzkoppe and the coast at Henties Bay (Marsh *et al.*, 1991*l*). Some are spectacular mica-rich mafic ultrapotassic rock-types, with >6 wt % K_2O at 8 wt % MgO (Thompson *et al.*, 2001*l*). Others differ little from dolerites petrographically but all have broadly similar and distinctive chemical compositions that can clearly be seen from their normalized multi-element patterns (Fig. 13b), which emphasize their steep REE patterns and relative enrichments in Ba, Rb, U, Th, Nb, Ta, Sr and P. The analysed Spitzkoppe lamprophyre FH129 is distinctive in having a high Pb/Ba ratio—a characteristic shared by the Spitzkoppe picrites (Fig. 13)—which may therefore indicate a localized trace-element feature in their source regions. Although the Spitzkoppe lamprophyre FH129 itself is clearly unsuitable in composition to generate the Spitzkoppe picrites simply by mixing in small amounts with a MORB-like progenitor (Fig. 13b), its compositional similarities to them are enough to suggest

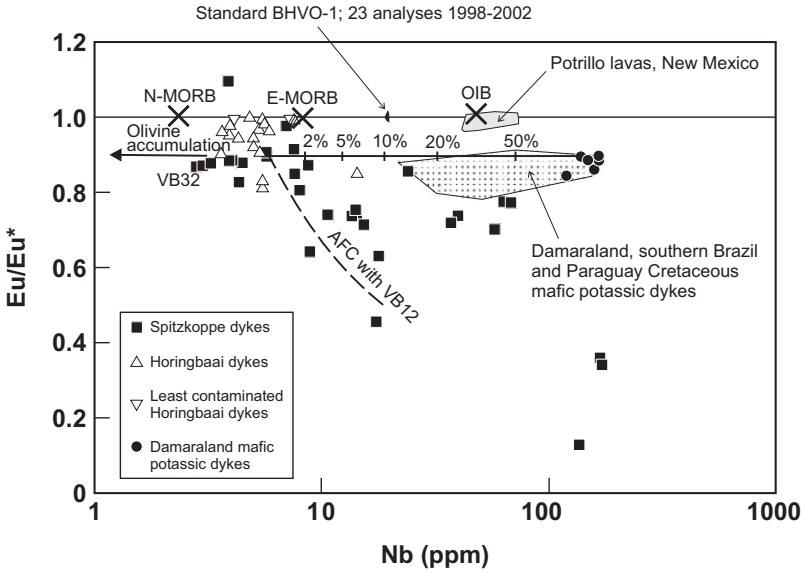

Fig. 14. Eu anomaly vs Nb for Spitzkoppe dykes and comparisons. MORB and OIB averages from Sun & McDonough (1989). Horingbaai dykes and Potrillo lavas from Thompson *et al.* (2001, 2005). Sources of Damaraland province mafic potassic dyke data are as for Fig. 13; Brazil and Paraguay field contains only data from Durham INAA or ICP-MS analyses, to eliminate inter-laboratory analytical differences (Gibson *et al.*, 1994, 1995*a*, 1995*b*, 1999, 2005, 2006; Thompson *et al.*, 1998).

that either lamprophyric melts or their SCLM sources were involved in the genesis of the picrites.

The clearest evidence that these Cretaceous lamprophyric rock-types in Namibia originated in veined and metasomatized SCLM sources comes from their close similarity to the Cretaceous lamprophyres and lamproites that occur associated with the Paraná flood basalts throughout southern Brazil and Paraguay (e.g. Gibson *et al.*, 1995*a*, 1995*b*, 2005). The exotic Sr, Nd, Pb and Os isotope ratios of the South American examples point clearly to their sources as geologically ancient SCLM veins (Gibson *et al.*, 1995*a*, 1995*b*, 2005; Carlson *et al.*, 1996). In contrast, the Sr, Nd and Pb isotopic ratios of the Namibian lamprophyres fall close to those of the most Mg-rich Spitzkoppe picrites VB11 and 32 (Figs 5 and 7). As the Namibian lamprophyres (especially FH129) are relatively rich in Sr, Nd and Pb, only a small input from their SCLM sources would be sufficient to dominate the Sr–Nd-Pb isotope ratios of the Spitzkoppe picrites, even if the latter were originally MORB-like Mg-rich melts from the underlying convecting mantle (see also Figs 14 and 16). Milner & le Roex (1996) and le Roex & Lanyon (1998) emphasized that the isotopic characteristics of the Cretaceous Namibian lamprophyres could best be explained if their veined and/or metasomatized SCLM mantle sources developed only shortly before the alkalic magmatism.

The Spitzkoppe picrites plot close to and slightly below the εNd–εHf mantle array in Fig. 6. In contrast, the dashed vectors in this diagram show how the peridotites forming ancient SCLM mostly plot far above the array (Pearson *et al.*, 2003). Such peridotites presumably form a substantial component of the SCLM beneath the granulite-facies sub-Damara lower crust. If so, ancient SCLM peridotites clearly played no significant role in the genesis of the Spitzkoppe picrites. Nevertheless, a minor component in the picrites derived from olivine-poor pyroxenitic SCLM veins is entirely consistent with the data in Fig. 6 because such veins plot scattered along the Mantle Array (Pearson & Nowell, 2004). Additionally, the lamproites and similar mafic potassic magmas that are generally supposed to be largely melts of SCLM mica-pyroxenite veins also plot along the Mantle Array in Fig. 6, extending to very low εNd and εHf ratios (Nowell & Pearson, 2003). Thus, the addition of a small amount of such melt to a MORB-like initial Spitzkoppe magma would affect its composition in the way seen in Fig. 6. This process would also not affect Os-isotope ratios of the Spitzkoppe magma significantly because Os is concentrated in mantle peridotites, rather than their olivine-poor veins (Hauri, 2002). Another scenario would be for the convecting mantle source of the picrites to incorporate wholesale some reactivated Thermal Boundary Layer mantle from the base of the sub-Spitzkoppe SCLM, including its population of veins (Thompson *et al.*, 2005).

Finally, the behaviour of Eu in the Spitzkoppe picrite dykes is consistent with this view of their origin. Figure 14 shows how the Eu anomaly (Eu/Eu*, where Eu* is the average of Sm and Gd abundances; all normalized to chondritic meteorites) can be determined very accurately and remains extremely close to 1·0 in average MORB

and OIB (Sun & McDonough, 1989) and in typical continental small-scale suites of basalts, such as the Holocene Potrillo lavas, USA (Thompson *et al.*, 2005). In contrast, virtually all the Spitzkoppe dykes—picrites to rhyolites—have small to large negative Eu anomalies. With model picrite VB19 as the starting composition, we used pMELTS to calculate an Eu anomaly curve for AFC involving local granite VB12, terminating when MgO fell to 5 wt %. This shows that a combination of fractional crystallization involving plagioclase separation with AFC can account for much of the Eu anomaly variation in this suite because likely crustal contaminants, such as granite, all have large negative Eu anomalies inherited from the processes that formed them. Unless the Spitzkoppe picrites fractionated from even more Mg-rich parents, AFC involving crust cannot be invoked to explain why they also have negative Eu anomalies.

The alternative explanation of this geochemical feature in the Spitzkoppe suite stems from the observation that in Fig. 14 the abundant Cretaceous REE-rich mafic potassic and associated lamprophyric dykes of Namibia, southern Brazil and Paraguay all have similar slightly negative Eu anomalies to VB32, even though they definitely have not precipitated plagioclase. This geochemical feature of the Spitzkoppe picrites could therefore also be derived from a small SCLM component in their source magmas, rather than crustal contamination, although the latter would subsequently progressively increase the negative Eu anomaly in the fractionated dyke melts. A mixing curve in Fig. 14 between picrite VB19 and 96SB30, a Cretaceous Mg-rich potassic dyke from Okenyenya (Thompson *et al.*, 2001), shows that the Spitzkoppe picrite compositions would have been very sensitive to addition of small amounts of such potassic melt. Variable degrees of mantle fusion during picrite genesis would also have generated melts with variable Nb contents and similar low Eu anomalies. This process may have contributed to the range of Nb abundances in Spitzkoppe dykes with only small negative Eu anomalies.

IMPLICATIONS FOR ETENDEKA IGNEOUS PROVINCE MAGMATISM

How are Spitzkoppe and Etendeka magmatism related?

The close spatial proximity of the HB–O dyke swarm to penecontemporaneous Etendeka lava outcrops, the Huab sill complex and Damara belt Cretaceous intrusive complexes (Fig. 1) has inevitably caused most of those who have written about this large igneous province (LIP) to suppose that all these comprise a single magmatic event (e.g. Erlank *et al.*, 1984; Marsh *et al.*, 1991, 1997, 2001; Duncan *et al.*, 1998; Ewart *et al.*, 1998*a*; Harris & le Roex, 1998). Trumbull *et al.* (2004*a*, p. 23) stated explicitly that: 'the (HB–O) dykes represent exposed feeders to a now-eroded southern extension of the Etendeka basalt field'.

The Etendeka lavas show considerable geochemical diversity and as a result they have been subdivided in terms of both magma types, with supposed genetic individuality, and lineages of compositions linked by fractional crystallization (e.g. Erlank *et al.*, 1984; Peate, 1997; Ewart *et al.*, 1998*a*, 2004*a*; Marsh *et al.*, 2001). The Etendeka tholeiitic basalt and andesite lavas appear to lack exposed comagmatic picrites; the picrite lavas at their base are distinctive geochemically and cannot be directly related to them (Ewart *et al.*, 1998*a*; Gibson *et al.*, 2000; Tuff *et al.*, 2005). The dominant southern Etendeka basalt—andesite lavas form a chemically defined group variously known as Tafelberg (Erlank *et al.*, 1984; Marsh *et al.*, 2001) or 'LTZ-L' (Ewart *et al.*, 1998*a*, 2004*a*)—equivalent to the Paraná Gramado lava group (Peate, 1997). A few geochemically similar basic dykes are found in the swarm west of Brandberg (Thompson *et al.*, 2001). Figure 3 shows that TiO_2 abundances in the non-picritic Spitzkoppe dykes are the same as in southern Etendeka low-Ti (Tafelberg/LTZ-L) lavas at equivalent MgO contents (Marsh *et al.*, 2001). Likewise, Fig. 8a shows that the CIPW norms of the main southern Etendeka Tafelberg lava group plot in a field amongst the more fractionated Spitzkoppe dykes, whereas the associated more mafic Tafelberg/LTZ-L dykes (Ewart *et al.*, 1998*a*; Thompson *et al.*, 2001) show the same distinctive trend as the Spitzkoppe basalt–intermediate dykes in this diagram.

Sr–Nd–Pb initial isotope ratios show comparable similarities between the Spitzkoppe dykes and Etendeka low-Ti lavas and associated dykes. On an initial εNd vs $^{87}Sr/^{86}Sr$ plot (Fig. 5), the field of the latter is bisected by both the variation trend for less Mg-rich Spitzkoppe dykes and our model AFC curve, using pMELTS with Damara granite VB12 as the contaminant. The associated acid lavas of the Etendeka igneous province, represented by the Goboboseb quartz latites (Ewart *et al.*, 1998*b*), have Sr–Nd initial isotopic ratios close to those of the Spitzkoppe rhyolite dykes (Fig. 5). Using only post-1985 Pb isotopic data, the Etendeka low-Ti basic lavas and dykes (Fig. 7) define a field remarkably like that of the Spitzkoppe picrite–basalt dykes but extending to lower $^{206}Pb/^{204}Pb$ ratios. A few Tafelberg and northern Etendeka Khumib–Kuidas lavas with the combination of relatively low $^{206}Pb/^{204}Pb$ (<18·0), $^{87}Sr/^{86}Sr$ (<0·708) and $^{143}Nd/^{144}Nd$ (<0·5124) were claimed by Ewart *et al.* (2004*a*, p. 85) to show Pb isotope variations: 'not consistent with crustal contamination'. Their Pb isotope trends are shown as fields labelled 'Southern LTZ lavas and dykes' in Fig. 7. It is clear that, although separated by 100–200 km, they are collinear with the trend defined by the Spitzkoppe picrites and Mg-rich basalts. The remarkable regular fall in MgO in

the dykes along the latter trend leaves little doubt that it is AFC-related (see also Fig. 10, where R^2 for $^{206}Pb/^{204}Pb$ vs MgO for such dykes is 0·97). Is it, therefore, really possible to be so certain that the parallel isotopic trends in some Etendeka lavas have nothing to do with crustal contamination of the magmas?

Erlank *et al.* (1984) and Ewart *et al.* (1998*a*) favoured alternative models in which the range of elemental and isotopic compositions of the Etendeka magmas was explained by: (1) the magmas being sourced, at least in part, from heterogeneous and partly enriched upper mantle areas, including the SCLM; (2) AFC-mixing processes in which upwelling mafic magmas had interacted with continental crust, respectively. However, each group of workers conceded that they could not rule out the other possibility based on the available data. If the intra-crustal and sub-crustal processes affecting the Spitzkoppe parental picrite magmas (summarized in Fig. 12) are applicable to the evolution of the Etendeka magmas in general, the results of our present study accord approximately with—and add detail to—those of Ewart *et al.* (1998*a*). Probably it should be expected that the very large-scale Paraná–Etendeka magmatic systems would have developed large-volume magmatic systems in the middle–upper crust and that mixing processes would have erased most or all traces of any previous interactions involving lower crust. Likewise, it is more a matter of faith than logic to distinguish between crustal and SCLM inputs into such flood-basalt magmatism using only Sr, Nd, Hf and Pb isotopes.

Early clinopyroxene precipitation and Paraná–Etendeka magma group classification

The evidence above that 'cryptic' clinopyroxene crystallized at approximately mid-crustal depths from the Spitzkoppe basic magmas at ~9 wt % MgO, and that AFC processes involving various crustal rock-types affected essentially all of these melts, has serious implications for the use of various elemental ratios in classifying these, and hence potentially all, Paraná–Etendeka magmas. Figure 15 shows three plots frequently used in this way (e.g. Erlank *et al.*, 1984; Marsh *et al.*, 1991, 2001; Peate, 1997; Ewart *et al.*, 1998*a*, 2004*a*) with members of the Spitzkoppe dyke suite plotted on them and coded for MgO content. The large changes in all these inter-element ratios along the Spitzkoppe dyke trend are obvious. Furthermore, pMELTS–AFC modelling produces exactly the same inter-element ratio changes (Fig. 15b) and shows that this effect would be extremely variable, depending on the precise crustal contaminant. The point made in Fig. 15 would be irrelevant if all researchers kept to the stricture emphasized by Trumbull *et al.* (2004*a*, p. 27), that these ratios will only remain constant in closed-system fractional crystallization involving exclusively olivine. That would rule out all magmas in the Spitzkoppe suite with MgO <9 wt % and also all more Mg-rich melts that had interacted with lower crust, leaving virtually none to classify!

Unfortunately, analyses of Paraná–Etendeka lavas and dykes with far less than 9 wt % MgO are routinely classified, and their ultimate sources discussed, using diagrams involving Ti, Zr and Y. For instance, Marsh *et al.* (2001, Table 1) listed some of the analyses they used in their classification of Etendeka magmas, including Tafelberg (6·8–3·4 wt % MgO), Albin (6·8–4·5 wt % MgO) and Esmeralda (5·7–3·6 wt % MgO). Likewise, Ewart *et al.* (2004*a*, fig. 5) plotted Etendeka 'basalts and dolerites' with MgO slightly below 2 wt % MgO, and Peate (1997, fig. 7) used the term 'basalt' to include Paraná samples with just over 2 wt % MgO.

Can geochemical signals from below the lithosphere be recognized in Paraná–Etendeka magmas?

The most recent account of Etendeka magmatism (Ewart *et al.*, 2004*a*, 2004*b*) included extensive discussion of Paraná–Etendeka magmatism in general. Ewart *et al.* (2004*a*) concluded that: 'the emerging Tristan plume entrained (old) subducted material in the Transition Zone region' of the convecting mantle, and that this is the main cause of the crust-like geochemical imprint in Paraná–Etendeka lavas. The thesis of Ewart *et al.* (2004*a*) is an application to continental magmatism of proposals that have been developed to explain geochemical characteristics of oceanic magmatism, especially in the South Atlantic region. Following Hart's (1984) identification of a large-scale isotopic anomaly in Southern Hemisphere mantle (inferred from its magmatic products), many researchers have claimed to identify the geochemical 'footprint' in these oceanic magmas of either ancient subducted sediments or delaminated ancient SCLM circulating within the convecting mantle. Gibson *et al.* (2005) recently summarized the magmatism of the Walvis Ridge, Rio Grande Rise and the islands of Tristan da Cunha, Inaccessible and Gough. They showed that shallow-mantle recycling of the SCLM metasomatized roots of several geochemically distinctive cratons in SW Africa and SE Brazil provided the most convincing explanation of the elemental and isotopic signatures of Cretaceous and subsequent pre-Recent oceanic basalts in the South Atlantic.

Figure 7 includes Pb-isotopic analyses of 79 Ma basalts from Deep Sea Drilling Project (DSDP) hole 525A, Walvis Ridge, erupted close to the Mid-Atlantic Ridge at that time (Gibson *et al.*, 2005, fig. 1). Their $^{206}Pb/^{204}Pb$ ratios are so low that it is clearly feasible to see much of the isotopic characteristics of Etendeka

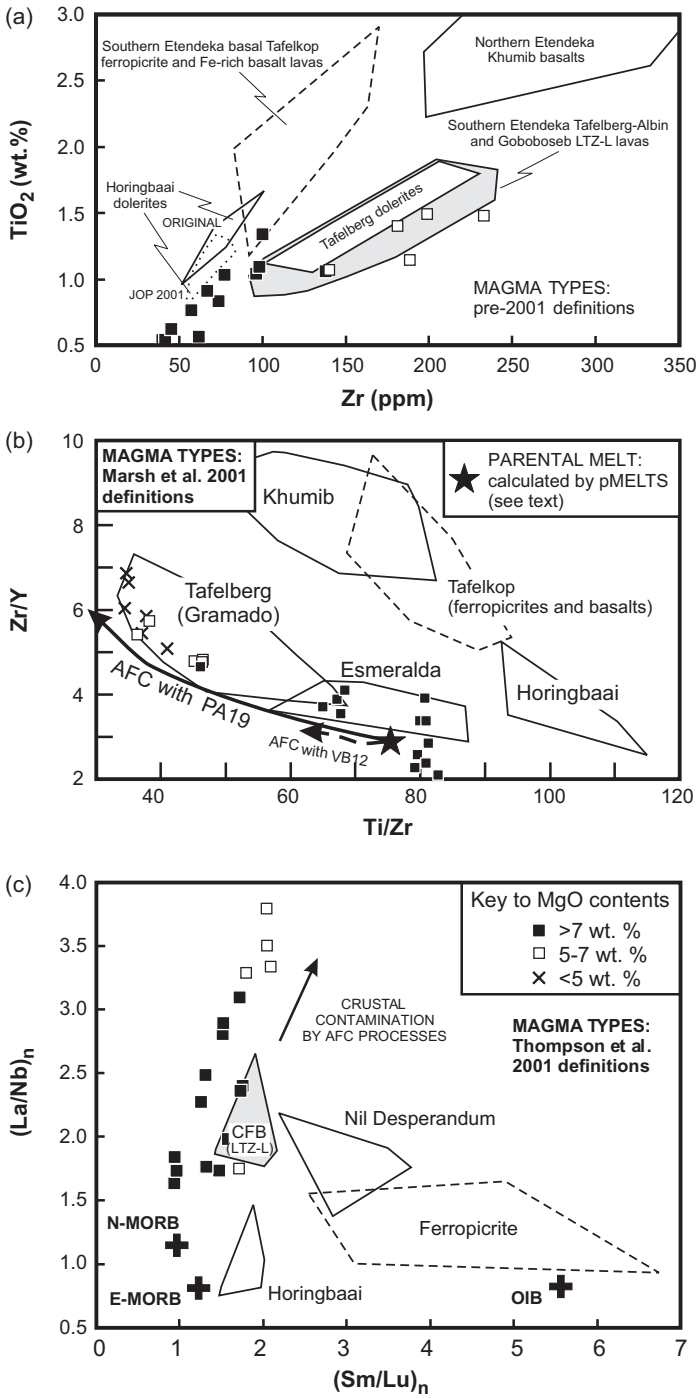

Fig. 15. Plots used in previous publications to classify Etendeka lavas (see text) with Spitzkoppe dyke data added. [See text for details of the pMELTS-AFC modelling trends on (b), shown as curved arrows.]

magmatism as inherited from convecting mantle sources, thus partially agreeing with the Ewart *et al.* (2004*a*) interpretation of Etendeka magmatism and earlier work on Paraná (e.g. Peate *et al.*, 1999). But do both these and other similar studies ignore the elephant in the room presented by the compositions of both continental crust and SCLM? The Paraná–Etendeka magmas clearly rose slowly through both these units, allowing extensive fractional crystallization to take place. To simplify the following argument, we shall concentrate only on the elements Nb and Pb. The $^{187}Os/^{188}Os$ ratios of Spitzkoppe picrite olivines (Table 4) are similar to those

of depleted N-MORB. If, as argued above, the Spitzkoppe parental melts at the top of the convecting mantle contained 15–20 wt % MgO, what might their Nb and Pb contents have been? Su & Langmuir (2003) listed the average Nb content of depleted MORB (MgO ~8 wt %) as 1·92 ppm. They gave no value for Pb but commented that their averages agreed well with those of Sun & McDonough (1989), who listed average Nb content of N-MORB (MgO ~8 wt %) as 2·33 ppm and Pb as 0·30 ppm. The Pb content is probably a maximum because elemental Pb determination at such abundances requires careful acid leaching of sample chips before analysis (N. Wittig & D. G. Pearson, unpublished data) and any global average will probably include some unleached samples. Therefore, allowing for the MgO difference between average MORB and picrite melts, we consider realistic Nb and Pb contents of the Spitzkoppe parental picrites to be 1·4 and 0·2 ppm, in agreement with the data of Kelley *et al.* (2005).

Attempting to derive average Nb and Pb contents for SCLM would be meaningless because it is demonstrably very heterogeneous (e.g. xenoliths and orogenic lherzolites) and hence variable in its fusibility. There is general agreement that the Cretaceous mafic potassic magmas of NW Namibia are the products of incipient SCLM fusion affecting its most fusible veins and patches (e.g. Milner & le Roex, 1996; le Roex & Lanyon, 1998; Thompson *et al.*, 2001). Therefore these are the best exposed representatives of potential contaminants of rising Spitzkoppe picritic melts. Average Nb and Pb contents for such rock-types (Fig. 13) are 150 and 7 ppm, respectively.

We argued above that the crust below Spitzkoppe lacks a mafic lower crust and, judging from Cretaceous palaeogeothermal gradients, was metamorphosed to granulite facies during Etendeka magmatism and had probably been so since the Archaean. The fusible parts of the exposed Damara Belt crust are dominated by granites (*sensu lato*) with very variable Nb contents of 3–40 ppm (averaging ~17) and Pb contents of 30–40 ppm (McDermott *et al.*, 1996; Jung *et al.*, 2003; this paper, Table 2). Although there are no obvious theoretical reasons why Nb contents should change in fusible rock-types within the middle or lower crust, Dickin (1981) showed that average Pb contents in Lewisian gneisses fall from 12 ppm in amphibolite-facies samples to 5 ppm in granulite-facies samples.

The import of these figures is that the rising Spitzkoppe parental melts from convecting mantle sources will travel through: (1) SCLM melting locally to a contaminant with ~100 times the Nb and 35 times the Pb content of the Spitzkoppe magmas at that depth; (2) overlying crust with much lower Nb contents, close to those of the (now fractionated) magmas; (3) lower crust with fusible rock-types similar to SCLM veins in Pb content but followed by higher crustal layers with Pb rising to ~200 times the original picrite values. Faced with rising through both SCLM and crust having such huge relative enrichments of both Nb (SCLM) and Pb (SCLM and crust), is it realistic for Peate *et al.* (1999), Ewart *et al.* (2004*a*) and others to suppose that any—let alone most—continental flood basalts rise from their convecting mantle sources, fractionate extensively and reach the surface without substantial modification of their Nb and Pb contents?

Figure 16 is a plot of Sr/Pb vs Nb/Nb* (defined in the legend) used by Ewart *et al.* (2004*a*) to argue their case for subducted ancient sediment in the convecting mantle sources of Paraná–Etendeka magmas. In this version the Walvis Ridge DSDP hole 525A basalts, Spitzkoppe dykes, pMELTS modelling and other data are added. If our analysis above of the SCLM Nb budget is correct, the overall SCLM average compositions of McDonough (1990) and Ionov (1996) marked in Fig. 16 are probably irrelevant. The averages for N-MORB and OIB (Sun & McDonough, 1989) and the fields for Tristan da Cunha and DSDP hole 525A lavas show that oceanic magmas in the South Atlantic diverge considerably in Nb/Nb* from typical MORB or OIB but less than most Spitzkoppe dykes. The fields for Cretaceous mafic potassic rock-types show very large variations in Nb/Nb* (0·4–2·6) within both the Paraná and Etendeka regions. If, as argued above, these Nb-rich SCLM melts dominated the Nb contents of picrite magmas rising through them (Gibson *et al.*, 1995*a*), it is unsurprising that the Spitzkoppe picrites have relatively low Nb/Nb* ratios that show no systematic correlation with MgO content, in contrast to the behaviour of other geochemical parameters in the dykes (Figs 5–7 and 10). A mixing curve in Fig. 16 between average N-MORB and Etendeka mafic potassic sample OKU-94-1 (le Roex & Lanyon, 1998) shows that the addition of only 1% of the latter shifts Nb/Nb* of N-MORB into the Spitzkoppe picrite range.

The two AFC curves calculated using pMELTS show that this process affects the plotted parameters extremely variably, depending on the crustal contaminant. The VB12/AFC model curve is similar in length and orientation to the elongation of the Esmeralda, Gramado and Tafelberg lava group fields given by Ewart *et al.* (2004*a*). Although the Spitzkoppe data broadly conform to this AFC model curve (Fig. 9), the scatter shown by the picrite data is repeated by the less Mg-rich dykes. This is as would be expected, if individual magma batches pursued individual paths through the Pb-rich continental crust.

The lesson from Spitzkoppe appears to be that such problems may be so complex as to be insoluble with certainty at present, unless there is access to complete extensive comagmatic suites, such as the one around Spitzkoppe, and much more knowledge of the composition of the lower crust throughout the region. This principle has

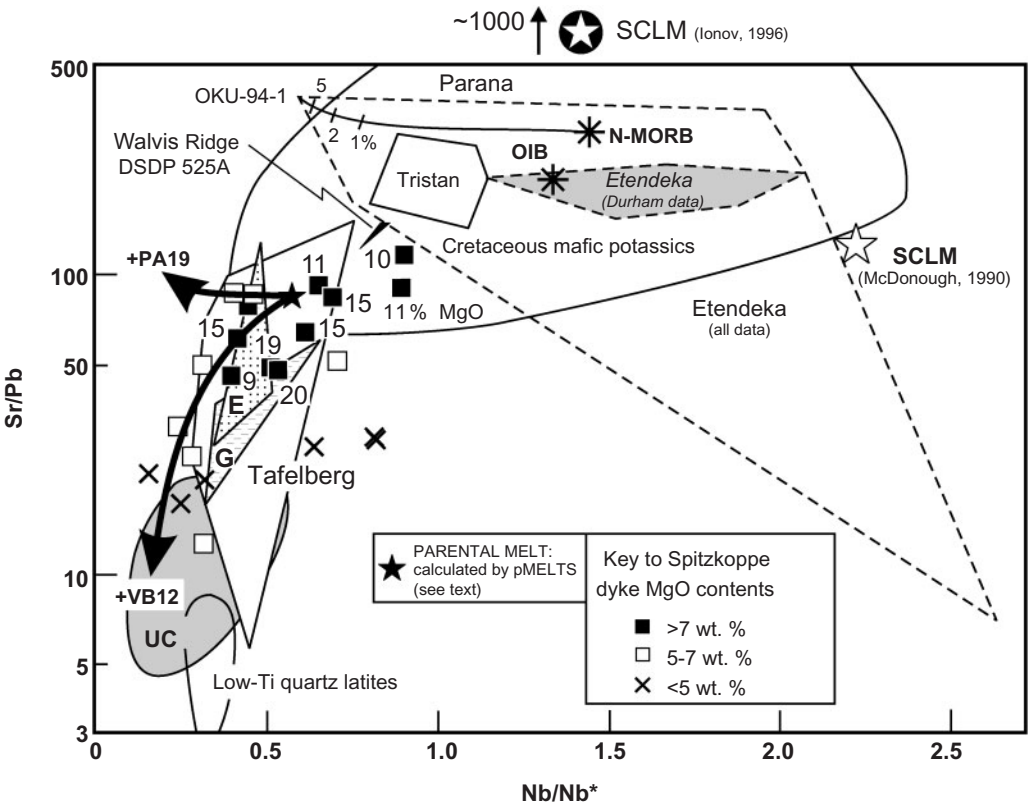

Fig. 16. Sr/Pb vs Nb/Nb* for southern Paraná–Etendeka lavas and dykes, after Ewart *et al.* (2004*a*, fig. 11a). Nb/Nb* was defined by Eisele *et al.* (2002) as $[Nb_N/\sqrt{(Th_N{*}La_N)}$, normalized to primitive mantle]. E, Esmeralda lavas; G, Gramado lavas; UC, upper crust. Spitzkoppe dyke data are coded according to their MgO contents. MgO values are marked beside most basalt–picrite points. AFC trends are modelled using pMELTS (see text for details) shown as curved arrows. Curved-outline fields are from Ewart *et al.* (2004*a*). Polygonal fields are drawn for data plotted by Ewart *et al.* (2004*a*) and in Fig. 13b. (See Fig. 13 for sources of Etendeka mafic potassic dyke data.)

been known for a long time (e.g. Moorbath & Thompson, 1980; Thompson *et al.*, 1982, 1986; Dickin *et al.*, 1984, 1987; Morrison *et al.*, 1985) and is regularly rediscovered and embellished (e.g. Baker *et al.*, 1996; Kent *et al.*, 2002; Yaxley *et al.*, 2004; Harlou *et al.*, 2006).

Acid magmas

The Spitzkoppe rhyolite dykes and granite (Harris, 1995; Frindt *et al.*, 2004*a*, 2004*b*; Trumbull *et al.*, 2004*b*), throw similar light on the genesis of acid and sub-acid magmas in the Paraná–Etendeka LIP. Erlank *et al.* (1984) considered that the large-scale Etendeka latites and quartz-latites were crustal melts. Subsequent studies have divided between emphasizing the concept that both these erupted rock-types and the substantial acid magmatism associated with the Damara belt Cretaceous intrusive centres were products of extensive AFC interaction between mafic magmas and continental crust (e.g. Ewart *et al.*, 1998*b*) and the alternative that the observed geochemical range of the acid magmas can be attributed to extensive crustal melting by the Cretaceous mafic magmas and variable mixing between these two contrasting components (e.g. Harris, 1995; Trumbull *et al.*, 2004*b*). As Harris (1995, p. 318) pointed out: 'The distinction between assimilation and crustal melting when the former exceeds 60–70% is probably one of semantics'. Our study adds detail to this picture in one case and emphasizes that the complexity in intermediate melt compositions caused by AFC within the lower–middle crust may be effectively disguised by a subsequent upper-crust geochemical 'overprint' in the acid residua. This may be the reason why Trumbull *et al.* (2004*b*) concluded, on the basis of Nd and O isotope data, that the crust below the Damara belt was relatively uniform laterally on a large scale.

SUMMARY

The ~132 Ma dyke swarm in the vicinity of Spitzkoppe, in the Damara Pan-African orogenic belt of western Namibia (Fig. 1), comprises dykes ranging continuously in composition from picrite (~20 wt % MgO) to rhyolite. Samples from the thickest (~10–20 m) picrite dykes have olivine phenocrysts that appear, from microprobe analyses, to be accumulative (Fig. 2). They also contain both small amounts of orthopyroxene and traces of biotite in their groundmasses (Table 1). Plagioclase phenocrysts join the

olivine in less Mg-rich basalt dykes and other phenocryst phases, such as clinopyroxene and Fe–Ti oxides, are confined to intermediate–acid dykes. Nevertheless, CaO and Sc variation in the dyke suite (Fig. 3) suggests that liquidus Ca-rich clinopyroxene precipitated from the melts when their MgO content reached ~9 wt %. This phenomenon can occur if fractional crystallization takes place at high pressures, and a plot of CIPW-normative di–hy–ol–ne-Q (Fig. 8) in the Spitzkoppe dykes with MgO >3 wt % suggests that the magmas may have fractionated at mid-crustal depths.

Variations in Sr, Nd, Hf and Pb isotope ratios within the dyke suite (Figs 5–7) show clearly that their fractional crystallization was under open-system conditions (AFC). For each radiogenic isotopic ratio, there is a good to excellent correlation with MgO content in parts of the dyke suite. These correlations indicate the likelihood that various crustal rock-types—some exposed at the present surface and others widely considered to form the sub-Damara-belt lower crust—were assimilated by the Spitzkoppe magmas. When all the measured isotopic ratios are plotted synoptically as functions of MgO (Fig. 10), it becomes clear that the isotopic nature of the inferred crustal contaminant changed systematically as a function of MgO. Thus, isotopic variation in the picrites and Mg-rich basalts is consistent with AFC processes involving a crustal end-member with Sr–Nd–Hf–Pb isotope ratios appropriate for intermediate to acid granulite-facies metamorphic rocks. Such rock-types are thought to be likely to form the lower sub-Spitzkoppe crust (Bauer *et al.*, 2000) and are indirectly 'sampled' by the distinctive Sr–Nd isotopic ratios of acid lavas in the nearby early Cretaceous sub-volcanic complex at Paresis (Mingram *et al.*, 2000). Likewise, the radiogenic isotope systematics of most of the basaltic–intermediate dykes (~9–3 wt % MgO; Table 3) point to an amphibolite-facies metamorphic (middle-crust?) end-member. Finally, the rhyolite dykes and two basalts appear to have interacted predominantly with crust Pb isotopically similar to the Damara belt rock-types exposed at the present surface and forming the local upper crust (e.g. Miller, 1983; McDermott *et al.*, 1989, 1996; McDermott & Hawkesworth, 1990).

The calculated densities of the dyke magmas fall progressively from picrite to rhyolite and this relationship, combined with the geochemical variation, leads to the concept that the sub-Spitzkoppe magmatic system was probably a stacked sequence of interconnected sill-like bodies, extending vertically throughout the sub-Spitzkoppe continental crust (Fig. 11). Episodic extension across the region tapped the magma reservoirs at varying depths, leading to the emplacement of the dyke swarm and also the contemporaneous Spitzkoppe granitic stocks.

The geochemistry of even the most Mg-rich picrites suggests that, although they lack significant crustal contamination, they nevertheless incorporate a small component from a source that was not the convecting upper mantle. Os isotopic ratios in the picrite olivines (Table 4) are at the low end of the MORB range (e.g. Gannoun *et al.*, 2004; Alard *et al.*, 2005). The easiest way to explain many other trace-element and isotopic ratios in the Mg-picrites is to envisage that they originated from the same convecting mantle source as MORB and subsequently, during uprise, interacted with partial melts from the same sort of metasomatized SCLM as formed the source of a suite of Early Cretaceous mafic potassic magmas emplaced sparsely throughout the southern Etendeka igneous province.

Petrogenetic modelling adapted and expanded the Adiabat_1ph version of the MELTS and pMELTS thermodynamically based algorithms (Smith & Asimow, 2005). Thus, the model began with only two input parameters: (1) the composition of the Depleted Mantle source proposed by McKenzie & O'Nions (1991, 1995); (2) the thermodynamic properties of the relevant components and minerals. Extensive trial-and-error calculations using pMELTS found a set of P–T conditions where this mantle generated a picrite melt with ~20 wt % MgO, which, after olivine fractionation, would evolve to compositions close to those of the less Mg-rich Spitzkoppe picrites. Further pMELTS fractionation modelling confirmed that mid-crustal pressures (most probably ~0·6 GPa; equivalent to ~24 km depth) were probably necessary to precipitate Ca-rich clinopyroxene at ~9 wt % MgO (Fig. 9). An expansion of the Adiabat_1ph software to model heat-balanced AFC processes can reproduce the essential features of a wide range of elemental and isotopic ratios within the Spitzkoppe dyke suite (e.g. Figs 5 and 14–16).

Finally, the processes deduced and modelled for the Spitzkoppe dyke suite appear also to help explain some geochemical features of the southern Paraná–Etendeka magmatism in general (Figs 15 and 16). The crucial wider message of this research is that elemental ratios widely used for classifying basic igneous rocks, and thought to reflect their mantle sources, become variable if either clinopyroxene fractionation or AFC processes involving continental crust (let alone both) take place. Thus, this study may contribute to the overall understanding of how the magmas of both Paraná–Etendeka and other continental large igneous provinces evolved. We show that the hot upwelling picrite parental melts—generated within the convecting upper mantle beneath such regions—become contaminated during their uprise through both SCLM and continental crust (and their extensive fractional crystallization within the latter) because of the huge disparities between the concentrations of key elements, such as Nb and Pb, in the parental picrites and the more fusible parts of both SCLM and crust.

ACKNOWLEDGEMENTS

The hospitality of the Damara people around Spitzkoppe made our sampling there a pleasure. Nick Marsh did us the substantial favour of analysing the major elements in the samples at Leicester University, and Dave Plant kindly found time on the SX-l00 microprobe at Manchester University. Jeremy Preston swiftly designed and produced a bespoke spreadsheet for using partial molar volumes to calculate melt densities. Mark Ghiorso and Paul Asimow generously allowed us to modify their MELTS code. Bruce Charlier facilitated the mass spectrometry at the Open University and provided substantial help and encouragement. The Director and staff of the Geological Survey of Namibia strongly encouraged this study and greatly facilitated its progress. The paper was immensely improved by the thoughtful and constructive comments of Andy Saunders, Chris Harris and an anonymous referee, plus the Herculean efforts of editor Gareth Davies.

SUPPLEMENTARY DATA

Supplementary data for this paper are available at *Journal of Petrology* online.

REFERENCES

Alard, O., Luguet, A., Pearson, N. J., Griffin, W. L., Lorand, J.-P., Gannoun, A., Burton, K. W. & O'Reilly, S. Y. (2005). *In situ* Os isotopes in abyssal peridotites bridge the isotopic gap between MORBs and their source mantle. *Nature* **436**, 1005–1008.

Asimow, P. D. (1997). A thermodynamic model of adiabatic melting of the mantle. PhD thesis, California Institute of Technology, Pasadena.

Asimow, P. D., Hirschmann, M. M., Ghiorso, M. S., O'Hara, M. J. & Stolper, E. M. (1995). The effect of pressure-induced solid–solid phase transitions on decompression melting of the mantle. *Geochimica et Cosmochimica Acta* **59**, 4489–4506.

Asimow, P. D., Dixon, J. E. & Langmuir, C. H. (2004). A hydrous melting and fractionation model for mid-ocean ridge basalts: application to the Mid-Atlantic Ridge near the Azores. *Geochemistry, Geophysics, Geosystems* **5**(1), Q01E16, doi:10.1029/2003GC000568.

Baker, J. A., Thirlwall, M. F. & Menzies, M. A. (1996). Sr–Nd–Pb isotopic and trace element evidence for crustal contamination of plume-derived flood basalts: Oligocene flood volcanism in western Yemen. *Geochimica et Cosmochimica Acta* **60**, 2559–2581.

Bauer, K., Neben, S., Schreckenberger, B., Emmermann, R., Hinz, K., Fechner, N., Gohl, K., Schluze, A., Trumbull, R. B & Weber, K. (2000). Deep structure of the Namibian continental margin as derived from integrated geophysical studies. *Journal of Geophysical Research* **105**, 25829–25853.

Baumgartner, M. C., le Roex, A. P. & Gurney, J. J. (2000). Mantle and crustal xenoliths from the Okenyenya lamprophyre diatreme: constraints on the upper mantle and lower crust beneath the Damara Belt, northwestern Namibia. *Communications, Geological Survey Namibia, Henno Martin Special Volume* **12**, 279–290.

Blundell, D. J., Hurich, C. A. & Smithson, S. B. (1985). A model for the MOIST seismic reflection profile, N. Scotland. *Journal of the Geological Society, London* **142**, 477–483.

Bowen, N. L. (1928). *The Evolution of the Igneous Rocks.*Princeton, NJ: Princeton University Press, 334 pp.

Carlson, R. W., Esperança, S. & Svisero, D. P. (1996). Chemical and Os isotopic study of Cretaceous potassic rocks from southern Brazil. *Contributions to Mineralogy and Petrology* **125**, 393–405.

Chauvel, C. & Blichert-Toft, J. (2001). A hafnium isotope and trace element perspective on melting the depleted mantle. *Earth and Planetary Science Letters* **190**, 137–151.

Christensen, N.I. & Mooney, W.D. (1995). Seismic velocity structure and composition of the continental crust: A global view. *Journal of Geophysical Research*, 100, 9761–9788..

Dickin, A. P. (1981). Isotope geochemistry of Tertiary igneous rocks from the Isle of Skye, NW Scotland. *Journal of Petrology* **22**, 155–189.

Dickin, A. P. (2005). *Radiogenic Isotope Geology*. Cambridge: Cambridge University Press, 492 pp.

Dickin, A. P., Brown, J. L., Thompson, R. N., Halliday, A. N. & Morrison, M. A. (1984). Crustal contamination and the granite problem in the British Tertiary Volcanic Province. *Philosophical Transactions of the Royal Society of London, Series A* **310**, 755–780.

Dickin, A. P., Jones, N. W., Thirlwall, M. F. & Thompson, R. N. (1987). A Ce/Nd isotope study of crustal contamination processes affecting Palaeocene magmas in Skye, NW Scotland. *Contributions to Mineralogy and Petrology* **96**, 455–464.

Duncan, A. R., Milner, S. C. & Jerram, D. A. (1998). *Field Excursion C4: Southern Etendeka volcanism, northwestern Namibia. IAVCEI International Volcanological Congress.* Cape Town: IAVCEI.

Eisele, J., Sharma, M., Galer, S. J. G., Blichert-Toft, J., Devey, C. W. & Hofmann, A. W. (2002). The role of sediment recycling in EM-1 inferred from Os, Pb, Hf, Nd, Sr isotope and trace element systematics of the Pitcairn hotspot. *Earth and Planetary Science Letters* **196**, 197–212.

Erlank, A. J., Marsh, J. S., Duncan, A. R., Miller, R. McG., Hawkesworth, C. J., Betton, P. J. & Rex, D. C. (1984). Geochemistry and petrogenesis of the Etendeka volcanic rocks from SWA/Namibia. *Special Publication of the Geological Society of South Africa* **13**, 195–245.

Ewart, A., Milner, S. C., Armstrong, R. A. & Duncan, A. R. (1998a). Etendeka volcanism of the Goboboseb Mountains and Messum igneous complex, Namibia. Part I: Geochemical evidence of Early Cretaceous Tristan plume melts and the role of crustal contamination in the Paraná–Etendeka CFB. *Journal of Petrology* **39**, 191–225.

Ewart, A., Milner, S. C., Armstrong, R. A. & Duncan, A. R. (1998b). Etendeka volcanism of the Goboboseb Mountains and Messum igneous complex, Namibia. Part II: Voluminous quartz latite volcanism of the Awahab magma system. *Journal of Petrology* **39**, 227–253.

Ewart, A., Marsh, J. S., Milner, S. C., Duncan, A. R., Kamber, B. S. & Armstrong, R. A. (2004a). Petrology and geochemistry of early Cretaceous bimodal continental flood volcanism of the NW Etendeka, Namibia. Part I: Introduction, mafic lavas and re-evaluation of mantle source components. *Journal of Petrology* **45**, 59–105.

Ewart, A., Marsh, J. S., Milner, S. C., Duncan, A. R., Kamber, B. S. & Armstrong, R. A. (2004b). Petrology and geochemistry of early Cretaceous bimodal continental flood volcanism of the NW Etendeka, Namibia. Part II: Characteristics and petrogenesis of the high-Ti latite and high-Ti and low-Ti voluminous quartz latite eruptives. *Journal of Petrology* **45**, 107–138.

Frindt, S., Haapala, I. & Pakkanen, L. (2004a). Anorogenic Gross Spitzkoppe granite stock in central western Namibia: Part I. Petrology and geochemistry. *American Mineralogist* **89**, 841–856.

Frindt, S., Trumbull, R. B. & Romer, R. L. (2004b). Petrogenesis of the Gross Spitzkoppe topaz granite, central western Namibia: a geochemical and Sr–Nd–Pb isotope study. *Chemical Geology* **206**, 43–71.

Gannoun, A., Burton, K. W., Thomas, L. E., Parkinson, I. J., van Calsteren, P. & Schiano, P. (2004). Osmium isotope heterogeneity in the constituent phases of mid-ocean ridge basalts. *Nature* **303**, 70–72.

Garcia, M. O. (1996). Petrography and olivine and glass chemistry of lavas from the Hawaii Scientific Drilling Project. *Journal of Geophysical Research* **101**, 11701–11713.

Garcia, M. O., Hulsebosch, T. P. & Rhodes, J. M. (1995). Olivine-rich basalts from the southwest rift zone of Mauna Loa volcano: implications for magmatic processes and geochemical evolution. In: Rhodes, J. M. & Lockwood, J. P. (eds) *Mauna Loa Revealed: Structure, Composition, History and Hazards*. Washington, DC: *Geophysical monograph, American Geophysical Union*, **92**, pp. 219–239.

Geological Survey of Namibia (1997). *Sheet 2114—Omaruru. 1:250 000 Geological Series*. Windhoek: Geological Survey of Namibia.

Ghiorso, M. S. & Sack, R. O. (1995). Chemical mass transfer in magmatic processes, IV, a revised and internally consistent thermodynamic model for the interpolation and extrapolation of liquid–solid equilibria in magmatic systems at elevated temperatures and pressures. *Contributions to Mineralogy and Petrology* **119**, 197–212.

Ghiorso, M. S., Hirschmann, M. M., Reiners, P. W. & Kress, V. C. (2002). The pMELTS: a revision of MELTS for improved calculation of phase relations and major element partitioning related to partial melting of the mantle to 3 GPa. *Geochemistry, Geophysics, Geosystems* **3**(5), doi: 10.1029/2001GC000217.

Gibson, S. A., Thompson, R. N., Leonardos, O. H., Turner, S. E., Mitchell, J. G. & Dickin, A. P. (1994). The Serra do Bueno potassic diatreme: a possible hypabyssal equivalent of the ultramafic alkaline volcanics in the Late Cretaceous Alto Paranaíba Igneous Province, SE, Brazil. *Mineralogical Magazine* **58**, 357–372.

Gibson, S. A., Thompson, R. N., Dickin, A. P. & Leonardos, O. H. (1995a). High-Ti and low-Ti mafic potassic magmas: key to plume–lithosphere interactions and continental flood-basalt genesis. *Earth and Planetary Science Letters* **136**, 149–165.

Gibson, S. A., Thompson, R. N., Leonardos, O. H., Dickin, A. P. & Mitchell, J. G. (1995b). The Late Cretaceous impact of the Trindade mantle plume: evidence from large-volume, mafic, potassic magmatism in SE Brazil. *Journal of Petrology* **36**, 189–229.

Gibson, S. A., Thompson, R. N., Leonardos, O. H., Dickin, A. P. & Mitchell, J. G. (1999). The limited extent of plume–lithosphere interactions during continental flood basalt genesis: geochemical evidence from Cretaceous magmatism in southern Brazil. *Contributions to Mineralogy and Petrology* **137**, 147–169.

Gibson, S. A., Thompson, R. N. & Dickin, A. P. (2000). Ferropicrites: geochemical evidence for Fe-rich streaks in upwelling mantle plumes. *Earth and Planetary Science Letters* **174**, 355–374.

Gibson, S. A., Thompson, R. N., Day, J., Humphris, S. E. & Dickin, A. P. (2005). Melt generation processes associated with the Tristan mantle plume: constraints on the origin of EM-1. *Earth and Planetary Science Letters* **237**, 744–767.

Gibson, S. A., Thompson, R. N. & Day, J. A. (2006). Timescales and mechanisms of plume–lithosphere interactions: $^{40}Ar/^{39}Ar$ chronology and geochemistry of alkaline igneous rocks from the Paraná–Etendeka large igneous province. *Earth and Planetary Science Letters* **251**, 1–17.

Gladczenko, T. P., Hinz, K., Edholm, O., Meyer, H., Neben, S & Skogseid, J. (1997). South Atlantic volcanic margins. *Journal of the Geological Society, London* **154**, 465–470.

Graham, D. W., Blichert-Toft, J., Russo, C. J., Rubin, K. H. & Albarède, F. (2006). Cryptic striations in the upper mantle revealed by hafnium isotopes in southeast Indian ridge basalts. *Nature* **440**, 199–202.

Green, R. W. E. (1983). Seismic refraction observations in the Damara orogen and flanking craton and their bearing on deep seated processes in the orogen. *Special Publication of the Geological Society of South Africa* **11**, 355–367.

Grove, T. L., Kinzler, R. J. & Bryan, W. B. (1992). Fractionation of mid-ocean ridge basalt (MORB). In: Morgan, J. P., Blackman, D. K. & Sinton, J. M. (eds) *Mantle Flow and Melt Generation at Mid-Ocean Ridges*. Washington, DC: *Geophysical monograph, American Geophysical Union*, **92**, pp. 281–310.

Harlou, R., Pearson, D. G., Davidson, J. P., Kamenetski, V. S. & Yaxley, G. M. (2006). Source variability and crustal contamination of the Baffin Island picrites—coupled Sr isotope and trace element study of individual melt inclusions. In: *16th Annual Goldschmidt Conference, Melbourne*, Abstract 0608026.

Harris, C. (1995). Oxygen isotope geochemistry of the Mesozoic anorogenic complexes of Damaraland, northwest Namibia: evidence for crustal contamination and its effect on silica saturation. *Contributions to Mineralogy and Petrology* **122**, 308–321.

Harris, C. & le Roex, A. (1998). *Field excursion C5: Mesozoic magmatism of northwestern Namibia. IAVCEI International Volcanological Congress*. Cape Town: IAVCEI.

Hart, S. R. (1984). A large-scale isotope anomaly in the Southern Hemisphere mantle. *Nature* **309**, 753–757.

Hauri, E. H. (2002). Osmium isotopes and mantle convection. *Philosophical Transactions of the Royal Society of London, Series A* **360**, 2371–2382.

Hauri, E. H., Gaetani, G. A. & Green, T. H. (2006). Partitioning of water during melting of the Earth's upper mantle at H_2O-undersaturated conditions. *Earth and Planetary Science Letters* **248**, 715–734.

Helz, R. T. (1980). Chemical and experimental study of the Ice Harbor member of the Yakima Basalt subgroup: evidence for intracrust storage and contamination. *EOS Transactions, American Geophysical Union* **61**, 68.

Hirschmann, M. M., Ghiorso, M. S., Wasylenki, P. D., Asimow, P. D. & Stolper, E. M. (1998). Calculation of peridotite partial melting from thermodynamic models of minerals and melts. I. Review of methods and comparisons with experiments. *Journal of Petrology* **39**, 1091–1115.

Ionov, D. A. (1996). Distribution and residence of lithophile trace element in minerals of garnet and spinel peridotites: an ICP-MS study. *Journal of Conference Abstracts* **1**, 278.

Jung, S., Mezger, K. & Hoernes, S. (2003). Petrology of basement-dominated terranes II. Contrasting isotopic (Sr, Nd, Pb and O) signatures of basement-derived granites and constraints on the source region of granite (Damara orogen, Namibia). *Chemical Geology* **199**, 1–28.

Kelley, K. A., Plank, T., Farr, L., Ludden, J. & Staudigel, H. (2005). Subduction cycling of U, Th and Pb. *Earth and Planetary Science Letters* **234**, 369–383.

Kent, A. J. R., Baker, J. R. & Wiedenbeck, M. (2002). Comtamination and melt aggregation processes in continental flood basalts: constraints from melt inclusions in Oligocene basalts from Yemen. *Earth and Planetary Science Letters* **202**, 577–594.

Kuritani, T., Kitagawa, H. & Nakamura, E. T. I. (2005). Assimilation and fractional crystallization controlled by transport process of crustal melt: implications from an alkali basalt–dacite suite from Rishiri Volcano, Japan. *Journal of Petrology* **46**, 1421–1442.

Le Bas, M. J. (2000). IUGS reclassification of the high-Mg and picritic volcanic rocks. *Journal of Petrology* **41**, 1467–1670.

Le Galle, B., Tshoso, G., Jourdan, F., Féraud, G., Bertrand, H., Tiercelin, J. J., Kampunzu, A. B., Modisi, M. P., Dyment, J. & Maia, M. (2002). $^{40}Ar/^{39}Ar$ geochronology and structural data from the giant Okavango and related mafic dyke swarms, Karoo igneous province, northern Botswana. *Earth and Planetary Science Letters* **202**, 595–606.

Le Maitre, R. W. (2002). *Igneous Rocks: A Classification and Glossary of Terms: Recommendations of the International Union of Geological Sciences Subcommission on the Systematics of Igneous Rocks*. Cambridge: Cambridge University Press.

le Roex, A. P. & Lanyon, R. (1998). Isotope and trace element geochemistry of Cretaceous Damaraland lamprophyres and carbonatites, northwestern Namibia: evidence for plume–lithosphere interactions. *Journal of Petrology* **39**, 1117–1146.

Lord, J., Oliver, G. J. H. & Soulsby, J. A. (1996). Landsat MSS imagery of a Lower Cretaceous regional dyke swarm, Damaraland, Namibia: a precursor to the splitting of Western Gondwana. *International Journal of Remote Sensing* **17**, 2945–2954.

Marsh, B. (2004). A magmatic mush column Rosetta Stone: the McMurdo Dry Valleys of Antarctica. *EOS Transactions, American Geophysical Union* **85**(47), 497–508.

Marsh, J. S., Erlank, A. J. & Duncan, A. R. (1991). Preliminary geochemical data for dolerite dykes and sills of the southern part of the Etendeka Igneous province. *Communications, Geological Survey of Namibia* **7**, 71–73.

Marsh, J. S., Harris, C. & Kirstein, L. (1997). Etendeka dykes, Namibia—relationship to Paraná–Etendeka lavas with implications. In: *Abstracts: IAVCEI International Volcanological Congress, Puerto Vallarta, Mexico*, p. 161.

Marsh, J. S., Ewart, A., Milner, S. C., Duncan, A. R. & Miller, R. McG. (2001). The Etendeka Igneous Province: magma types and their stratigraphic distribution with implications for the evolution of the Paraná–Etendeka flood basalt province. *Bulletin of Volcanology* **62**, 464–486.

McDermott, F. & Hawkesworth, C. J. (1990). Intracrustal recycling and upper-crust evolution: a case study from the Pan-African Damara mobile belt, central Namibia. *Chemical Geology* **83**, 263–280.

McDermott, F., Harris, N. B. W. & Hawkesworth, C. J. (1989). Crustal reworking in southern Africa: constraints from Sr–Nd isotope studies in Archaean to Pan-African terrains. *Tectonophysics* **161**, 257–270.

McDermott, F., Harris, N. B. W. & Hawkesworth, C. J. (1996). Geochemical constraints on crustal anatexis: a case study from the Pan-African Damara granitoids of Namibia. *Contributions to Mineralogy and Petrology* **123**, 406–423.

McDonough, W.F. (1990) Constraints on the composition of the continental lithospheric mantle. *Earth and Planetary Science Letters*, 101, 1–18.

McKenzie, D. & O'Nions, R. K. (1991). Partial melt distributions from inversion of rare earth element concentrations. *Journal of Petrology* **32**, 1021–1091.

McKenzie, D. & O'Nions, R. K. (1995). The source regions of ocean island basalts. *Journal of Petrology* **36**, 133–159.

Miller, R. McG. (1983). The Pan-African Damara orogen of South West Africa/Namibia. *Special Publication of the Geological Society of South Africa* **11**, 431–515.

Milner, S. C. & le Roex, A. P. (1996). Isotope characteristics of the Okenyenya igneous complex, northwestern Namibia: constraints on the composition of the early Tristan plume and the origin of the EM1 mantle component. *Earth and Planetary Science Letters* **141**, 277–291.

Milner, S. C., le Roex, A. P. & O'Connor, J. M. (1995). Age of Mesozoic rocks in northwestern Namibia, and their relationship to continental breakup. *Journal of the Geological Society, London* **152**, 97–104.

Mingram, B., Trumbull, R. B., Littman, S. & Gerstenberger, H. (2000). A petrogenetic study of anorogenic felsic magmatism in the Cretaceous Paresis ring complex, Namibia: evidence for mixing of crust and, mantle-derived components. *Lithos* **54**, 1–22.

Moorbath, S. & Thompson, R. N. (1980). Strontium isotope geochemistry and petrogenesis of the Early Tertiary lava pile of the Isle of Skye, Scotland and other basic rocks of the British Tertiary Igneous Province: an example of magma–crust interaction. *Journal of Petrology* **21**, 295–321.

Moorbath, S., Powell, J. L. & Taylor, P. N. (1975). Isotopic evidence for the age and origin of the grey gneiss complex of the southern Outer Hebrides. *Journal of the Geological Society, London* **131**, 213–222.

Morrison, M. A., Thompson, R. N., Dickin, A. P. & Gibson, I. L. (1985). Geochemical evidence for complex magmatic plumbing during development of a continental volcanic centre. *Geology* **13**, 581–584.

Nowell, G. M. & Pearson, D. G. (2003). Lu–Hf and Re–Os systematics of lamproites: constraints on their petrogenesis. *Geophysical Research Abstracts* **5**, 05458.

Nowell, G. M., Kempton, P. D., Noble, S. R., Fitton, J. G., Saunders, A. D., Mahoney, J. J. & Taylor, R. N. (1998). High precision Hf isotope measurements of MORB and OIB by thermal ionisation mass spectrometry: insights into the depleted mantle. *Chemical Geology* **149**, 211–233.

Pearson, D. G. & Nowell, G. M. (2004). Re–Os and Lu–Hf isotope constraints on the origin and age of pyroxenites from the Beni Bousera peridotite massif: implications for mixed peridotite–pyroxenite melting models. *Journal of Petrology* **45**, 439–455.

Pearson, D. G. & Woodland, S. J. (2000). Carius tube digestion and solvent extraction/ion exchange separation for the analysis of PGEs (Os, Ir, Pt, Pd, Ru) and Re–Os isotopes in geological samples by isotope dilution ICP-mass spectrometry. *Chemical Geology* **165**, 87–107.

Pearson, D. G., Canil, D. C. & Shirey, S. B. (2003). Mantle samples included in volcanic rocks, xenoliths and diamonds. In: Holland, H. D. & Turekian, K. K. (eds) *Treatise in Geochemistry, Volume 2*. Amsterdam: Elsevier, pp. 171–275.

Pearson, D. G., Irvine, G. J., Ionov, D. A., Boyd, F. R. & Dreibus, G. E. (2004). Re–Os isotope systematics and Platinum Group Element fractionation during mantle melt extraction: a study of massif and xenolith peridotite suites. *Chemical Geology* **208**, 29–59.

Peate, D. W. (1997). The Paraná–Etendeka province. In: Mahoney, J. J. & Coffin, M. F. (eds) *Large Igneous Provinces: Continental, Oceanic and Planetary Flood Volcanism*. Washington, DC: *Geophysical monograph, American Geophysical Union*, **100**, pp. 217–245.

Peate, D. W., Hawkesworth, C. J., Mantovani, M. S. M., Rogers, N. W. & Turner, S. P. (1999). Petrogenesis and stratigraphy of the high Ti/Y Urubici magma type in the Paraná flood basalt province and implications for the nature of 'Dupal'-type mantle in the South Atlantic region. *Journal of Petrology* **40**, 451–473.

Reiners, P. W., Neilson, B. K. & Ghiorso, M. S. (1995). Assimilation of felsic crust by basaltic magma: thermal limits and extents of crustal contamination of mantle-derived magmas. *Geology* **23**, 563–566.

Rudnick, R. L. & Gao, S. (2003). The crust. In: Holland, H. D. & Turekian, K. K. (eds) *Treatise in Geochemistry, Volume 3*. Amsterdam: Elsevier, pp. 1–64.

Saal, A. E., Rudnick, R. L., Ravizza, G. E. & Hart, S. R. (1998). Re–Os isotope evidence for the composition, formation and age of the lower continental crust. *Nature* **393**, 58–61.

Saal, A. E., Hart, S. R., Shimizu, N., Hauri, E. H., Layne, G. D. & Eiler, J. M. (2005). Pb isotopic variability in melt inclusions from the EMI–EMII–HIMU mantle end-members and the role of the oceanic lithosphere. *Earth and Planetary Science Letters* **240**, 605–620.

Scherer, E. E., Cameron, K. L., Johnson, C. M., Beard, B. L., Barovich, K. M. & Collerson, K. D. (1997). Lu–Hf geochronology applied to dating Cenozoic events affecting lower crustal xenoliths from Kilbourne Hole, New Mexico. *Chemical Geology* **142**, 63–78.

Seth, B., Kröner, A., Mezger, K., Nemchin, A. A., Pidgeon, R. T. & Okrusch, M. (1998). Archaean to Neoproterozoic magmatic events in the Kaoko belt of NW Namibia and their geodynamic significance. *Precambrian Research* **92**, 341–363.

Smith, P. M. & Asimow, P. D. (2005). Adiabat.1ph: a new public front end to the MELTS, pMELTS and pHMELTS models. *Geochemistry, Geophysics, Geosystems* **6**(1), doi: 10.1029/2004GC000816.

Smith, P. M., Asimow, P. D. & Stolper, E. M. (2003). Thermodynamic modelling of melting in chemically heterogeneous mixtures of peridotite and pyroxenite. *Geochimica et Cosmochimica Acta* **67**, A440.

Spera, F. J. & Bohrson, W. A. (2004). Open-system magma chamber evolution: an energy-constrained geochemical model incorporating the effects of concurrent eruption, recharge, variable assimilation and fractional crystallization (EC-E'RAχFC). *Journal of Petrology* **45**, 2459–2480.

Su, Y. & Langmuir, C. H. (2003). Global MORB chemistry compilation at the segment scale. PhD thesis, Columbia University.

Sun, S. S. & McDonough, W. F. (1989). Chemical and isotope systematics of oceanic basalts: implications for mantle compositions and processes. In: Saunders, A. D. & Norry, M. J. (eds) *Magmatism in the Ocean Basins. Geological Society, London, Special Publications* **42**, 313–345.

Thompson, R. N. (1972). The 1-atmosphere melting patterns of some basaltic volcanic series. *American Journal of Science* **272**, 901–932.

Thompson, R. N. (1974). Primary basalts and magma genesis. I. Skye, north-west Scotland. *Contributions to Mineralogy and Petrology* **45**, 317–341.

Thompson, R. N. (1982). Magmatism of the British Tertiary Volcanic Province. *Scottish Journal of Geology* **18**, 49–107.

Thompson, R. N. (1987). Phase-equilibria constraints on the genesis and magmatic evolution of oceanic basalts. *Earth-Science Reviews* **24**, 161–210.

Thompson, R. N. & Gibson, S. A. (2000). Transient high temperatures in mantle plume heads inferred from magnesian olivines in Phanerozoic picrites. *Nature* **407**, 502–506.

Thompson, R. N., Esson, J. & Dunham, A. C. (1972). Major element chemical variation in the Eocene lavas of the Isle of Skye, Scotland. *Journal of Petrology* **13**, 219–253.

Thompson, R. N., Dickin, A. P., Gibson, I. L. & Morrison, M. A. (1982). Elemental fingerprints of isotopic contamination of Hebridean Palaeocene mantle-derived magmas by Archaean sial. *Contributions to Mineralogy and Petrology* **79**, 159–168.

Thompson, R. N., Morrison, M. A., Dickin, A. P. & Hendry, G. L. (1983). Continental flood basalts—arachnids rule OK? In: Hawkesworth, C. J. & Norry, M. J. (eds) *Continental Basalts and Mantle Xenoliths*. Glasgow: Shiva, Nantwich, pp. 158–185.

Thompson, R. N., Morrison, M. A., Dickin, A. P., Gibson, I. L. & Harmon, R. S. (1986). Two contrasting styles of interaction between basic magmas and continental crust in the British Tertiary Volcanic Province. *Journal of Geophysical Research* **91**, 5985–5997.

Thompson, R. N., Gibson, S. A., Mitchell, J. G., Dickin, A. P., Leonardos, O. H., Brod, J. A. & Greenwood, J. C. (1998). Migrating Cretaceous–Eocene magmatism in the Serra do Mar alkaline province, SE Brazil: melts from the deflected Trindade mantle plume? *Journal of Petrology* **39**, 1493–1526.

Thompson, R. N., Morrison, M. A., Hendry, G. L. & Parry, S. J. (1984). An assessment of the relative roles of crust and mantle in magma genesis: an elemental approach. *Philosophical Transactions of the Royal Society of London, Series A* **310**, 549–590.

Thompson, R. N., Gibson, S. A., Dickin, A. P. & Smith, P. M. (2001). Early Cretaceous basalt and picrite dykes of the southern Etendeka region, NW Namibia: windows into the role of the Tristan mantle plume in Paraná–Etendeka magmatism. *Journal of Petrology* **42**, 2049–2081.

Thompson, R. N., Ottley, C. J., Smith, P. M., Pearson, D. G., Dickin, A. P., Morrison, M. A., Leat, P. T. & Gibson, S. A. (2005). Source of the Quaternary alkalic basalts, picrites and basanites of the Potrillo Volcanic Field, New Mexico, USA—lithosphere or convecting mantle? *Journal of Petrology* **46**, 1603–1643.

Trumbull, R. B., Vietor, T., Hahne, K., Wackerle, R. & Ledru, P. (2004a). Aeromagnetic mapping and reconnaissance geochemistry of the Early Cretaceous Henties Bay–Outjo dyke swarm, Etendeka igneous province, Namibia. *Journal of African Earth Sciences* **40**, 17–29.

Trumbull, R. B., Harris, C., Frindt, S. & Wigand, M. (2004b). Oxygen and neodymium isotope evidence for source diversity in Cretaceous anorogenic granites from Namibia and implications for A-type granite genesis. *Lithos* **73**, 21–40.

Tuff, J., Takahashi, E. & Gibson, S. A. (2005). Experimental constraints on the role of garnet pyroxenite in the genesis of high-Fe mantle plume derived melts. *Journal of Petrology* **46**, 2023–2058.

Ulmer, P. (1989). The dependence of the Fe^{2+}–Mg cation-partitioning between olivine and basaltic liquid on pressure, temperature and composition. *Contributions to Mineralogy and Petrology* **101**, 261–273.

Villiger, S., Ulmer, P. & Müntener, O. (2007). Equilibrium and fractional crystallisation experiments at 0·7 GPa; the effect of pressure on phase relations and liquid compositions of tholeiitic magmas. *Journal of Petrology* **48**, 159–184.

Whitehead, K., le Roex, A., Class, C. & Bell, D. (2002). Composition and Cretaceous structure of the upper mantle beneath the Damara Mobile Belt: evidence from nephelinite-hosted peridotite xenoliths, Swakopmund, Namibia. *Journal of the Geological Society, London* **159**, 307–321.

Wigand, M., Schmitt., A. K., Trumbull, R. B., Villa, I. M. & Emmermann, R. (2003). Short-lived magmatic activity in an anorogenic subvolcanic complex: $^{40}Ar/^{39}Ar$ and ion microprobe U–Pb zircon dating of the Erongo, Damaraland, Namibia. *Journal of Volcanology and Geothermal Research* **2715**, 1–21.

Workman, R. K. & Hart, S. R. (2005). Major and trace element composition of the depleted MORB mantle (DMM). *Earth and Planetary Science Letters* **231**, 53–72.

Yaxley, G. M., Kamenetsky, V. S., Kamenetsky, M., Norman, M. D. & Francis, D. (2004). Origins of compositional heterogeneity in olivine-hosted melt inclusions from the Baffin Island picrites. *Contributions to Mineralogy and Petrology* **148**, 426–442.

Zhang, Z., Mahoney, J. J., Mao, J. & Wang, F. (2006). Geochemistry of picritic and associated basalt flows of the Western Emeishan flood basalt province, China. *Journal of Petrology* **47**, 1997–2019.

APPENDIX

Several experimentally calibrated algorithms have been proposed for predicting the crystallization of basaltic and associated melts. The MELTS (Ghiorso & Sack, 1995), pMELTS (Ghiorso *et al.*, 2002) and pHMELTS (Asimow *et al.*, 2004) algorithms solve for thermodynamic equilibrium between silicate liquid and solid phases. Adiabat_1ph (Smith & Asimow, 2005) is a text-based front-end to the (pH)MELTS family of algorithms—meaning MELTS, pMELTS and pHMELTS—that can simultaneously calculate trace-element and isotopic ratios and was employed here. MELTS and pMELTS may be used with anhydrous or water-saturated systems whereas pHMELTS (Asimow *et al.*, 2004), an extension of the models in which trace amounts of water are partitioned into nominally anhydrous minerals (e.g. olivine), can only be used for melting calculations.

The original release of Adiabat_1ph (Smith & Asimow, 2005) included a 'source-mix' function for one-off calculation of a new bulk composition from two sources. A later development was a 'flux-melting' mode in which the source region could be enriched at each calculation step. The new AFC functionality is an extension of this mode, in that the thermal as well as chemical effect of the added material is constrained and solid phases may be fractionated simultaneously. Similarly, although Smith & Asimow (2005) described many geologically plausible thermodynamic paths, such as isobaric, isentropic and isochoric, there had not been any user-demand for isenthalpic calculations. Recently we have enabled the isenthalpic mode, so that heat-balanced assimilation in an evolving magma chamber may be modelled, like the calculations described by Reiners *et al.* (1995). The scheme they used alternated between solution of a simple heat-balance equation for addition of crustal material, which used MELTS output as its input, and an fO_2 buffered fractional crystallization step performed with the MELTS software so that the equilibrium phase compositions and relevant thermodynamic quantities were updated for the new bulk composition and P–T conditions. Shortly after the Reiners *et al.* study, Asimow and Ghiorso completed modifications to the original MELTS model of Ghiorso & Sack (1995) that allowed isentropic or isenthalpic constraints to be imposed directly (Asimow, 1997). Asimow *et al.* (1995) compared 'isentropic' melting calculations approximated using an iterative procedure analogous to that of Reiners *et al.* (1995) with the isentropic decompression path predicted by the newly adapted MELTS algorithm. Asimow *et al.* (1995) found that both methods produced identical results and there is no doubt that a repeat of the Reiners *et al.* (1995) calculations using the isenthalpic MELTS function would do likewise.

The implementation of isenthalpic calculations is essentially that of the GUI version of MELTS, as maintained by M. S. Ghiorso (see http://melts.ofm-research.org/index.html), which is in turn similar to the method used for isentropic calculations (Asimow *et al.*, 1995). At a given pressure, an isothermal calculation involves minimizing the Gibb's free energy of the assemblage, whereas an isentropic calculation requires enthalpy minimization and an isenthalpic one employs entropy maximization. It should be noted that, as no compensation is made for gravity, isenthalpic calculations should really only be performed at constant pressure. Reiners *et al.* (1995) performed their calculations at equally spaced temperatures, at each stage solving for the amount of assimilant added. Conversely, in both the GUI version of MELTS and the Adiabat_1ph front-end, a user-specified mass of solid (or liquid) is added and the MELTS algorithm returns the new temperature. However, the ways in which the initial conditions for the assimilant are specified differ in the details. Calculation of the initial enthalpy requires knowledge of both the temperature and the phase assemblage. In the GUI version of MELTS the user must list phase and end-member proportions, which will usually be inferred from microprobe analyses and estimates of modal abundance. In Adiabat_1ph the initial state of the assimilant is one that has been saved from a previous simulation for the given bulk composition, run to sub-solidus conditions. The difference in the predicted initial enthalpy calculated by either method is insignificant compared with that related to the uncertainty in the ambient temperature of the surrounding crust.

As currently formulated, it is not possible for (p)MELTS calculations that fix the total enthalpy to be simultaneously fO_2 buffered, as this would imply that oxygen entering or leaving the system carried no heat. This problem also exists for calculations along an isentrope or isochore. Instead, we have added an option to approximate fO_2-buffering in such situations. The procedure used for each incremental AFC step can therefore be summarized as follows: 1 g of material (equilibrated at 500°C) was added to the system and the composition and total enthalpy were adjusted accordingly. Next, pMELTS was run isenthalpically, with the fO_2 unbuffered, to determine the equilibrium outcome of this crustal addition. Then an extra equilibration step re-established the fO_2 buffer for the newly constrained P, T conditions and updated the reference enthalpy for any net change in oxygen content. Any resultant solid phases were discarded from the system and the liquid became the starting point for the next increment of added crust. This alternation between closed- and open-system behaviour is similar to that used by Reiners *et al.* (1995), and is also comparable with the way melt extraction is handled in most geochemical models of adiabatic ('isentropic') decompression melting, including Adiabat_1ph.